Swansea University
Prifysgol Abertawe

Preparation of Thin Film Silver Nanoparticles for Nanocatalysis Purposes: Deposition, Patterning and Etching

By

Ishraq A. Obaid

A DISSERTATION

Presented to the College of

Engineering at Swansea University

In Partial Fulfilment of the Requirements

For the Master Degree of Science

Major: Nanotechnology to Nanoscience

Under the Supervision of Professor Owen J. Guy

Swansea/United Kingdom

September 2015

747340@swansea.ac.uk

TO MY DEAR FATHER IN THE OTHER WORLD:

I love you and I would never forget you, I'm really sure that you are happy with me now.... I have achieved what you wished for me all your life.

My God.... Have mercy on my father and give him a place in the paradise.

Amen...

Your sincere daughter

Ishraq

Contents

Acknowledgements 5
Abstract 6
Chapter 1 7
Introduction 7
1.1. Background 8
1.2. The main characteristics of silver: 13
1.3 Examples of some common nanocatalysts 15
1.3.1. Microreactor for catalyst testing 15
1.3.2. Reusable Catalysts 16
1.3.3. Photocatalysts 16
1.4. The Research Overview 17
Chapter 2 18
Mechanisms of Films Preparation Applied to Design Nanostructured Features 18
2.1. Introduction 19
2.2. The most common metals and substrates for catalysts Composition 20
2.2.1. Silver (Ag) 20
2.2.2. Copper–Silver (Cu+Ag) 21
2.2.3. Silver-supported alumina ($Ag+Al_2O_3$) 21
2.2.4. Gold (Au) 22
2.2.5. Platinum and ceria ($Pt+CeO_2$) 23
2.2.6. Magnetic nanoparticles 24
2.2.7. Nickel (Ni) 24
2.2.8. Silicon (Si) 25
2.2.9. Cobalt (Co) 25
2.3. Conventional Deposition Techniques 26
2.1.1. Growth of metal nanocatalysts by magnetron sputtering: 27
2.1.2. Growth of nanometal catalyst by sol–gel technique: 29
2.2. Nanostructures Fabrication Techniques: 29
2.2.1. Electron Beam Lithography 30
2.2.2. Nanoimprint Lithography NIL 32
2.2.3. Substrate Conformal Imprint Lithography SCIL 36
2.3. Etching Process 37

2.3.1. Wet etching ... 37
2.3.2. Dry Etching ... 39
2.4. Lift-Off Finishing Method ... 40
2.5. Damascene lift-off process ... 41
2.6. Conclusion ... 41
Chapter 3 ... 42
Manufacturing Of Nanostructured Ag-Dots by EBL Technique ... 42
3.1. Introduction ... 43
3.2. Materials and methods ... 44
3.3. Results and Discussion ... 51
3.4. Conclusion ... 61
Chapter 4 ... 63
Manufacturing of nanostructured Features by SCIL technique ... 63
4.1. Introduction ... 64
4.2. Materials and methods ... 65
4.3. Results and Discussion ... 72
4.4. Conclusion ... 76
Chapter 5 ... 77
Conclusion and Recommendations ... 77
5.1. The Conclusion ... 78
5.2. Future Research ... 79
5.3. Future Work ... 79
References ... 81
List of Figures ... 93
List of Tables ... 94

Acknowledgements

First, I would like to acknowledge my supervisor Dr. Owen J. Guy. His support and guidance led me to not only new scientific experience but also the way of thinking and dealing with problems as a scientist. I would like to honestly thank Dr. Jone E. Evans, Dr. Gareth J. Blayney, and Dr. Kelly D. Walker for their efforts and advice in my research. I also warmly thank my kind family, especially my husband Rafid, my sons Hussein & Ala'a, and my daughters Tuqa, Teeb & Rahma for their patience and support along the period of my study. I would not have achieved this far without their emotional and moral support,

I am also grateful to my dear Mum and siblings: Osama, Afrah & Meelad for their prayers and encouragement. I gratefully thank my best friends Bukola, Sana'a, Nadiyah and Zeena for their advice and guidance. I acknowledge all the members in Centre of Nano Health CNH at Swansea University for their friendly welcoming along the research duration.

Finally, I sincerely thank the Iraqi government and Iraqi Cultural Attaché in London for their financial support and provide me the opportunity to complete my higher education abroad.

Ishraq Abbodi Fadhil Obaid

Al-Qadissiyah University/ College of Education

Physics Department

Al-Diwaniyah/ Iraq

Abstract

Silver is a chemical element symbolized by Ag with atomic number 47. It is one of other elements in a group called noble or transition metals within the periodic table (ruthenium, rhodium, palladium, silver, osmium, iridium, platinum, and gold). It possesses the highest electrical and thermal conductivity, and the best reflectivity of other metals. These abundant properties of silver make it an ideal candidate to use as a catalyst in oxidation reactions.

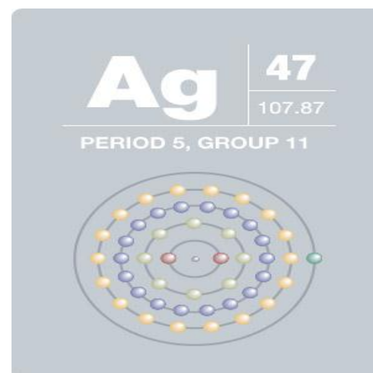

Nanotechnology has advanced enormous industries and scientific fields. In that respect, Ag is one of the materials that exploited by nanotechnology in various domains such as medicine, antibacterial products, photonics and also catalysis applications. Innovative methods for nanocatalysts synthesis have yielded a significant progress by modifying the surface properties of nanoparticles and, consequently, to promote their catalytic performance. Catalysis reactions are substantially influenced by the particles size, shape, structure, as well as the support and catalyst materials.

The main aim of this research is to deposit Ag thin films by physical vapour deposition PVD system/ DC magnetron sputtering as an initial investigation to study the optimal deposition technique, and the appropriate film thickness to create arrays of nanodots imprinted by Electron Beam Lithography EBL, which would eventually be used in nanocatalysts domains. The second goal of this research is to experience imprinting nanostructures by using Substrate Conformal Imprint Lithography SCIL technique, and compare the obtained results with the EBL results in terms of efficiency and time.

The results reveal that the optimised thickness of the Ag thin film is larger than 10nm and the created features are remarkably influenced by the dose exposure during the EBL imprinting. Additionally, in terms of silver deposited onto silicon dioxide SiO_2, lift-off method with diluted photoresist C1%PMMA yields high uniformity features than wet etching process. Nanostructure patterns created by SCIL technique deliver more encouraging yield in terms of features number imprinted on larger area within a shorter time comparing with EBL results.

Chapter 1

Introduction

1.1. Background

The general definition of a catalyst is a substance that motivates reactants to undergo a transition to products of a chemical reaction without itself undergoing a permenat change or being consumed during this reaction process. Recently, nanotechnology has revolutionised markets and scientific fields and, consequently, new catalysts materials and fabrication methodshave developed as a result of this modern technology.

Catalysts are typically exploited to increase a reaction speed through kinetic processes where the thermodynamic properties of the system remain constant. The main mechanism of how a catalyst acts is one of three states either it can reduce the activation energy of the system, efficiently performs as an initiator and pulls the reactants close together, or produces unequally yield rate for the reactions of more than two products (Chaturvedi, Dave & Shah, 2012).

Catalysts of nanomaterials, also called nanocatalysts, are substantially advanced industries, which involve the use of metallic nanoparticles as catalysts for a diversity of organic and inorganic processes. Nanoscale particles possess a large surface area-to-volume ratio which contributes significant physicochemical properties for catalysts with high reaction activity, 100% selectivity, long term stability and cost effective when compared with their bulk materials (Tian, Zhou, Sun, Ding & Wang, 2007).

Generally, catalysts are categorized into three key structures: homogeneous, heterogeneous and enzymatic catalysts. For homogeneous catalysis, the catalyst materials form as a colloidal solution of transition metal nanoparticles, which are uniformly dispersed in different media of solvents, organic or aqueous solutions. These colloidal solutions must be chemically stable to prevent nanoparticles aggregation and also to get appropriate recyclable catalysts. Basically, the reason for using transition metal colloids to engineer efficient catalysts is because of presenting a large number of atoms on the surface of the nanoparticles in terms of high surface area to volume ratio (Narayanan, 2005). While, heterogeneous catalysis reactions are fabricated differently by supporting transition metal nanoparticles (catalyst) in various substrates. Three major methods are used to prepare

heterogeneous nanocatalysts: 1. Lithographic techniques to fabricate nanostructures. 2. Nanoparticles adsorption on substrate surfaces. 3. Grafting nanoparticles on support materials (Narayanan, 2005).

Pure substrates are usually not active for many chemical reactions owing to the lack of the active species (Chen et al., 2011). Therefore, various chemical compounds are employed to design catalysts such as metals, metal sulphides and metal oxides which possess the ability to modify and accelerate a reaction by reducing the activation energy of the entire system. However, using extensive quantities of metal-based catalysts for different reactions is generally expensive and might negatively affect the human health and the environment. Accordingly, it is desirable to lessen their amounts because nanoscaled structures endow a substantially high surface area to volume ratio which advances the catalytic activity of the nanocatalysts (Moshfegh, 2009). Furthermore, other studies have shown that overall active surface area is not the only factor which influences the catalysts' function but also particles size, shape, porosity and separation between the catalyst features (Grothausmann et al., 2011). The major challenge with the nanoparticles NPs is their tendency to aggregate and producing unstable products. To confront this problem, a dispersion process has been exploited to prepare a media or support of high surface area which extremely leads to improve the catalyst function (Moshfegh, 2009). Thus, the support selectivity is the critical factor which broadly affects the distribution, formation, and dispersion of the viral species in catalytic oxidation processes (Chen et al., 2011). Depending on the supported nanomaterials, each support material possesses the characteristic properties for individual applications. Accordingly, changing a support substance may entirely vary the catalyst properties in terms of increase or inhibit the catalytic activity (Bhosale & Bhanage, 2015). The present study deals with silver metal properties and its essential role in advancing nanocatalyst industries for different disciplines. Therefore, it is necessary to report some of the supports that commonly used to prepare Ag-based nanocatalysts such as graphene, carbon nanotubes (CNT), TiO2, Al2O3, SiO2, mesoporous silica, zeolites, tungsten oxide, polymers, aerogel matrix and carbon support substances. These support materials and others containing Ag are substantially beneficial in particular promotion of the heterogeneous catalytic reactions (A. Bhosale & M.Bhanage, 2015).

Numerous nanomaterials play an efficient role in many chemical transformations, such as oxidation of hydrocarbons, hydrogenation dehydrogenation and redox reactions. These nanomaterials significantly alter a catalysis reaction as a function of their size, shape, structure and support materials (Bhatt, et al., 2015). Tables 1, 2, 3, and 4 present some catalysis reactions and their dependence on support materials, shape, catalysts materials and size, respectively.

Size dependent catalysis: It is well known that nanoparticles refer to miniaturised structures of nanoscaled dimensions and this reduction drastically alters their electronic properties. This phenomenon can be illustrated by referring to the reduction in density of states DOS of outer electrons and the spatial path length, which restricts the electronic motion, with size shrinkage. Thus, the electronic properties of metal nanoparticles are influenced by their size which consequently affects the work function of the particle surface. The main purpose of reducing the size of a catalyst particle is to enlarge the surface area of the active components exposed to the reactants and then specifically minimize the catalyst cost per function (Moshfegh, 2009). Bhatt et al. investigate the size dependent of TiO2, SnO2 and CeO2 support materials on their catalytic activation energy, they deduce that the catalytic activation energy of these materials minimises with decreasing particles size. This is an indication to the capability of nanoparticles to efficiently enhance any chemical reaction (Bhatt, Pratap, & Jha, 2015).

Shape dependent catalysis: It is evidenced that in addition to size influenced catalysis, the shape of nanocrystals can endow a considerable key role in their catalytic selectivity and activity. Narayanan stated in 2005 that tetrahedral PtNPs showed the lowest activation energy (high catalytic energy), where the cubic PtNPs gave the highest value. However, the spherical nanoparticles possessed a catalytic activity of moderate (Narayanan, 2005).

Structure dependent catalysis: The common materials structures are single crystal, thin films, polycrystals, nanoparticles and powder. It has been found that the activation energy of a catalysis reaction is strongly influenced by the catalyst structure, such reactions known as structure sensitive reactions. A good example of this kind of reaction is ammonia synthesis, which appears a high sensitivity to crystallographic planes (Moshfegh, 2009). Another observation presented that

nanoparticles of spherical structures reveal a more reliable catalytic performance than thin films and nanowires (Bhatt, et al., 2015).

Material dependent catalysis: The same investigation by Bhatt et al. Can be mentioned here as an example. It has been reported that the TiO2 nanoparticles have the lowest catalytic activation energy which indicates that the TiO2 nanostructures can be exploited in catalysis reactions according to their powerful catalytic activities. Accordingly, the nanomaterials examined in their study showed that SnO2 has a beneficial role in specific catalysis reactions whereas for others not adequately effective but introduced the least chemical activity. Moreover, CeO2 catalytic material showed an intermediate value of the activation energy between TiO2 and SnO2 (Bhatt, et al., 2015).

Table 1 shows a few AgNPs/ supports to advance catalysis reactions

Ag/support material nanocatalysts	Chemical reaction	Activity	Ref.
Ag/ branched polyethyleneimine derivatives	Reduction	Active	A.Bhosale and M. Bhanage, 2015
Ag/GNP graphene nanoplatelets	Oxygen reduction	Active	A.Bhosale and M. Bhanage, 2015
Ag/ tungsten oxide	Selective oxidation of cyclohexene to adipic acid	Active	A.Bhosale and M. Bhanage, 2015

Table 2 shows PtNPs as an example of shape dependent catalysis

Shape dependent platinum-based nanocatalysts	Catalytic activity	Atoms fraction	Ref.
Tetrahedral PtNPs	Very active	High	Narayanan, 2005
Spherical PtNPs	Moderately active	intermediate	Narayanan, 2005
Cubic PtNPs	Low activity	small	Narayanan, 2005

Table 3 shows (gold/ceria/silica) as an example of materials dependent catalysis

Material dependent metal-based nanocatalysts	Reaction type/ rate	Particle size (nm)	Ref.
$Au/CeO_2/HMS$	CO oxidation	High activity/ 18.8nm	Ren et al., 2012
$Au/CeO_2/SBA\text{-}15$		Intermediate activity/ (3.7, 6.2nm)	
$Au/CeO_2/KIT\text{-}6$		Low activity/ 5.5	

Table 4 shows some available examples of size dependent catalysis

Size dependent metal-based nanocatalysts	Reaction type/ rate	Particle size (nm)	Ref.
Au entities	Selective oxidation of styrene by dioxygen	(~1.4,<2)	Moshfegh, 2009
Ir/WO_3	Selective catalytic reduction of NO by CO	1–1.5	Moshfegh, 2009
Nano-sized Ag/TiO_2 particles	Methyl Orange decomposition	14.1	Moshfegh, 2009
Ag/TiO_2	Textile dye : Acid red 88 decomposition	10–20	Moshfegh, 2009
TiO_2 nanotube layers loaded with Ag and Au nanoparticles	Acid Orange decomposition	10 ± 2	Moshfegh, 2009
Ag/SiO_2	Methyl Red dye decomposition	19 ± 6	Moshfegh, 2009
Ag/ZnO	Methyl Orange decomposition	20–50	Moshfegh, 2009
Ag/TiO_2	H_2 generation	100	Moshfegh, 2009

Catalytic oxidation is commonly used as an efficient way to limit air pollution (Sekine, 2002). In this field, noble metals (Pt, Au, Ag, Ru and, Pd) are utilised as promising supports to eliminate the formation of formaldehyde products such as methane and other carbon compounds (Zhang et al., 2005). Silver (Ag) has been reported in several catalysis applications due to its cheapness and significant efficiency in

various oxidation processes at low temperatures (Scirèet al., 2009). Interestingly, the nature of the support materials strongly affects the activity of silver-based catalysts (Lin, et al., 2001). Silver-based catalysts are commonly altered by manipulating silver species into diverse conditions such as metallic silver particles with oxygen or isolated (Ag+) ions on the surface of silica SiO_2 or titania TiO_2 substrates (Scirè et al., 2010). Consequently, Ag nanoparticles-based catalysts have attracted major attention in industries due to their efficacy in developing novel catalysts for broad purposes, for instance, oxidation, hydrogenation and environmental applications (Liu et al., 2008).

Many forms of noble metal active species have been exploited to fabricate silica surfaces as model catalysts to improve the catalytic function and identify the relationship between structure and activity of nanocatalysts (Wang & Liu, 2011) and (Escamilla-Perea et al., 2010). Silica is commonly used as a catalyst support owing to its special properties, for instance, high thermal stability, high surface area, inert chemical behaviour and the porosity of the matrix. These characteristics induce generating natural nucleation sites for crystallization which widely adopted in the field of adsorption and separation catalytic reactions (Hansen et al., 2011).

1.2. The main characteristics of silver:

Recently, silver nanoparticles have received great attention due to their efficient exhibition in developing modern catalysts for extensive purposes, such as oxidation, hydrogenation and environmental applications (Pârvulescu et al., 2010)

The metal silver (Ag) has many advantages over other metals when used in catalysis, for example:

a) It has an extremely excellent reflectivity and low polarization splitting for the infrared (IR) region and bellow to 400 nm of the spectrum;

b) It is absolutely inactive in variable values of PH in aqueous solutions with the absence of oxidizing agents or coordination compounds (ligands).

On the other hand, using Ag layers has a disadvantage which is their readiness to be tarnished at the ambient conditions and so gives insufficient reflectivity at wavelengths below 400 nm (Rizzo, Tagliente, Alvisi & Scaglione, 2001). Table 5 shows some important characteristics of silver with respect to other elements in the same group of the periodic table.

Practically, the morphology of Ag thin films is influenced by the fabrication method and the film thickness. For example, Ag thin films produced by a vapour deposition technique are shown significant differences in terms of their thicknesses when they are deposited under variable evaporation time (Rakocevic, et al, 2008).

Table 5 Comparison of silver properties with respect to gold and copper (Choi & Hess, 2014)

	Cu	Ag	Au
Atomic number	29	47	79
Group	11	11	11
Period	4	5	6
Atomic mass	63.5	107.9	197
Crystal structure	fcc	fcc	fcc
Atomic radius (pm)	135	160	135
Bond length (pm)	272	290	288
Electron configuration	[Ar] $3d^{10}$ 4 s^1	[Kr] $4d^{10}$ 5 s^1	[Xe] $5d^{10}$ 6 s^1
Resistivity (μΩ cm)	1.7	1.6	2.2
Self- Diffusivity (cm^2/s at 1000 K)	1.67E-09	1.07E-08	6.15E-09
Wave length of reflectance >85% (nm)	591	300	560
Electron work function (eV)	4.65	4.26	5.1
Electronegativity	1.9 (Pauling); 1.75 (Allrod Rochow)	1.93 (Pauling); 1.42 (Allrod Rochow)	2.54 (Pauling); 1.42 (Allrod Rochow)
Melting point (K)	1357.75	1234	1337.73
Enthalpy of fusion (kJ/mol)	13.01	11.3	12.55
Enthalpy of atomization (kJ/mol at 25°C)	338.9	284.5	364
Formation enthalpy of metal hydride crystal (kJ/mol)	CuH: 87 ± 17	AgH: 86 ± 19	AuH: 67 ± 19
Atomization enthalpy of metal hydride crystal (kJ/mol)	467 ± 17	417 ± 19	519 ± 19
Lattice energy (kJ/mol)	CuH: 1254 (thermochemical cycle) or 828 (calculated) CuH_2: 2941(calculated)	AgH: 941 (calculated)	AuH: 1033(calculated)

1.3 Examples of some common nanocatalysts

1.3.1. Microreactor for catalyst testing

Basically, a microreactor can be described as a microchannels system/chip in which the reaction materials will flow and react. The flow of the reactants within the microchannels is usually laminar, resulting in expected and well-controlled flow displays. The residence time of the gas existed in the catalyst bed is normally low owing to the micro-scale dimensions of the channels which can lead to obtain high space velocities (Henriksen, et al., 2009).

The microreactors are designed as analytical tools for catalysts analyses. The term 'catalyst analysis' involves catalytic activity measurements, apparent activation energy, turnover frequency, and surface area, in consequence of temperature programmed desorption and tests with transformation rate that varies with altering the temperature and gas phase stoichiometry. The high sensitivity of the reactor makes it especially compatible for major catalytic activity investigations of model catalysts with low surface areas (Henriksen, et al., 2009).

Microreactors have been proved to show vast benefits compared to common macroscaled reactors. The temperature of a microreactor can be adjusted quickly and easily due to the tiny dimensions. Because of the high surface area-to-volume ratio, a significant increase of heat transfer from and to the reaction zone is observed. This decreases the thermal gradient rate for the system and helps to get precise control of temperature, even for harshly exothermic interactions (Kolb & Hessel, 2004). Additionally, the small dimensions of such chemical machinery enhance mass transfer as well as lessen concentration gradients. Slight thermal and concentration gradients are advantageous when settling kinetic statistics. As a result, parameters of reactions that take place in small volumes, such as residence time, pressure and flow rate, can be controlled easily. Moreover, the microscale size of this type of reactors promisingly enhances the safety of use for explosive materials and importantly cuts down the consumption of gas during the chemical reaction. Finally, by employing micro-fabrication techniques, it becomes possible to integrate sensors and heaters simultaneously into microreactors (Henriksen, et al., 2009).

1.3.2. Reusable Catalysts

Although many studies have been done on nanocatalysts, a challenge of preparing reliable recyclable metal nanocatalysts still remains. To tackle this issue, a novel method is currently embraced which imply to metal nanoparticles immobilized on solid supports such as inorganic spheres or polymer resins, to ensure a complete catalysts separation from the product mixtures at the end of the reaction. However, the reactants movement within the liquid to the catalysts and also their transport within the supports can limit the reaction rate as the transport level to the catalyst surfaces will decrease with increasing the size of the entire catalyst (Shin, et al., 2009). Correspondingly, both the activity and the selectivity of suspended nanocatalysts could advance further if used miniaturized supports. In fact, it is easily to separate the suspended solid catalysts from the products by centrifugation or filtration, however, there are catalyst bodies with dimensions larger than about 3μm. Thus, smaller bodies are problematic to be separated and required advanced nanocatalysts of a magnetic core and a catalytic shell. Magnetically reused nanocatalysts permit the catalysts to be recycled appropriately when applying an exterior magnetic field. Many endeavours have been tried to synthesize noble-metal deposited magnetic materials such as Fe_3O_4 and Fe_2O_3 (Zhang, et al., 2006).

Monitoring a nanocatalyst during reuse set reaction to evaluate problems, could be happened like leaching or shape/size variation, is enormously important to design an optimal recyclable catalyst (Roucoux, Schulz & Patin, 2002). In the same field of study, Hariprasad and Radhakrishnan reported in 2010 that embedding magnetic metal nanoparticles within a polymer matrix effectively inhibits aggregation, and facilitates long-term storage of these nanocomposite films which adds a great relevance for recyclable catalysts (Hariprasad & Radhakrishnan, 2010).

1.3.3. Photocatalysts

A photoelectronic process is based on the electron excitation in a semiconductor substance by absorption a light energy higher than the energy of its band gap which induces the formation of electron-hole (e-h) pairs. In the field of photocatalysis, generation of (e-h) pairs is commonly identified to be any chemical reaction induced by a solid where an external electromagnetic field with wavelengths in the UV-visible region is applied. Photocatalysts are conventionally synthesise of solid oxide

semiconductors (Philippot & Serp,2013). Interestingly, Titanium dioxide (TiO_2) is considered as an excellent candidate for photocatalysts in enormous applications. The major advantages of TiO_2 are: its ability to be chemically stabile under harsh environments when exposed to basic and acidic compounds; it is nontoxic material; its highly oxidizing power and it is relatively cheap. These characteristics have induced employing it for various photocatalytical applications. TiO_2 can be found in three diverse crystalline modifications: brookite, rutile, and anatase. Among these crystals, anatase has the top overall catalytic activity. The high oxidization effect of TiO_2 helps to advance its efficacy in decomposition reactions of organic and inorganic composites at too low concentrations. The TiO2 photocatalytic behaviour can be exploited for self-sterilization, self-cleaning surfaces and decomposing atmospheric pollution (Ohama, & Van Gemert, 2011).

1.4. The Research Overview

The main purpose of this research is depositing silver thin films by physical vapour deposition PVD system with etching endeavours, and also some reasons and suggestions will be proposed to tackle several potential issues that could occur in Substrate Conformal Imprint Lithography SCIL technique.

A general literature review has explained various fields in terms of fabrication processes, nanoimprinting techniques, finishing approaches such as etching and lift-off scenarios and also several metals of commonly used in catalysts synthesis will be included in Chapter 2.

Two different methods for creating silver nanoparticles AgNPs on silicon dioxide SiO2 wafers using Electron Beam Lithography EBL technique will be described in Chapter 3, in detail.

Employing Substrate Conformal Imprint Lithography SCIL technique to imprint silicon nanowires SNWs as a preliminary study for future research expected to be tested in CNH will be comprehensively explained in Chapter 4.

Lastly, a final conclusion and recommendations for future plans depending on the obtained insights in Chapter 3 and 4 will be briefly proposed in Chapter 5.

Chapter 2

Mechanisms of Films Preparation Applied to Design Nanostructured Features

2.1. Introduction

Development of new techniques to improve catalysts performance is an active area of research. Nanotechnology is an essential approach to establish modern industries in different disciplines such as electronics, environment, medicine and catalysis. Interestingly, catalysis reactions and catalysts fabrication techniques are significantly attracted more attention and advancement. Generally, fabrication techniques of catalysts can be classified into two strategies conventional and unconventional fabrication technologies.

Conventional techniques for nanofabrication are top-down techniques which commercially available and extensively employed in catalysts industries. Photolithography and scanning beam lithography such as focused ion beam and electron beam lithography are the most commonly adopted in the conventional fabrication techniques. These techniques are relatively expensive and low quality, and also largely restricted to flat surfaces in semiconductor fabrication. Additionally, these types of manufacturing techniques can damage substrates by exposing to high-energy radiation, relatively high temperatures and corrosive etchants. (Gates et al., 2005)

Unconventional approaches present alternative routes for photolithographic nanofabrication methods which include both the bottom-up and top-down manipulation strategies. They involve printing, embossing, and molding which are examples of top-down approaches, as well as, scanning probe lithography (SPL) and self-assembly processes which combine the both strategies by using top-down methods to fabricate templates to guide the bottom up assembly mechanisms (Gates et al., 2005). The previous techniques offer great opportunities to pattern various features on non-planar surfaces, especially, smooth and curved surfaces, and can be used over large areas. These approaches possess the prospect to be the most efficient and economical methods for nanostructured device manufacturing. Unconventional routes are also practically much easier to apply than conventional techniques and therefore, motivate a wide range of nanoscience and nanotechnology disciplines, especially those related to applied physics and electrical engineering which historically weak, to be explored (Gates et al., 2005).

It is necessary to mention that there are numerous types of catalysts materials such as metalic, organic and nonorganic composites. In this cahapter the only metalic materials and their catalytic properties have been covered, briefly. Physical and chemical vapour deposition methods have been mentioned. Additionally, some advanced techniques in fabrication nanoscaled features have be clarified. Finally, etching and lift-off processes utilised to produce the final appearance of patterened features have been described at the end of this chapter.

2.2. Common metals and substrates for catalysts Composition

2.2.1. Silver (Ag)

Silver is one of the most active elements in oxidation catalysts (Nagy, Mestl & Schlögl, 1999); as it is a vital composition for ethene epoxidation industries. Nevertheless, silver can be employed as a catalyst for reduction processes like selective hydrogenation of unsaturated aldehydes (BRON et al., 2005).

Separation of hydrogen H_2 molecules on clean silver surfaces is anticipated by theoretical calculations (Eichler, et al, 1998) to be an endothermic interaction. Zhukov et al. stated that H2 molecules do not adsorb on single crystal silver surfaces at the ambient conditions (Zhukov, Rendulic & Winkler, 1996). The solubility of H_2 in silver is actually low over a wide range of pressure and temperature (Lewis, 1990). Thus, chemical processes that requiring the existence of adsorbed hydrogen atoms on the surface are not possible on silver. Consequently, silver alone is not desirable as a hydrogenation catalyst; however, it is exploited in dehydrogenation reaction (Hohmeyer et al., 2010).Yet, incorporation of silver into palladium for catalysis purposes enhances the hydrogenation properties which revealed that incorporation these metals together advances the catalytic selectivity (Zhang, et al., 2000). Claus' group demonstrated that higher surface pressure produces higher selectivity (Wei et al., 2013).

2.2.2. Copper–Silver (Cu+Ag)

Un-promoted copper–silver bimetallic catalysts arranged by successive impregnation in aqueous solution show developed action and selectivity with respect to un-promoted silver catalysts for the epoxidation of ethylene to ethylene oxide (EO) (Linic, et al., 2004). Cu–Ag bimetallic catalysts upgraded with Cs and/or Cl are more active and more selective for ethylene epoxidation than promoted silver catalysts. Higher selectivity is not so much connected with lower activity. These incorporate working at low ethylene transformation and utilizing monolith supported catalysts to give uniform, rapid contact times. Briefly, the addition of Cu to produce a bimetallic structure advanced both activity and selectivity (JANKOWIAK & BARTEAU, 2005), while adding Cs had moderately little impact on action vs. increasing selectivity; and addition of Cl pointedly reduced action vs. enhancing selectivity of both Ag and Cu–Ag bimetallic catalysts (Linic & Barteau, 2003).

2.2.3. Silver-supported alumina (Ag+Al_2O_3)

Silver-supported alumina (Al_2O_3) catalysts have been researched. The planning of these catalysts was performed either by impregnation of the metal salts (Lippits, Gluhoi & Nieuwenhuys, 2007), precipitation and altered precipitation, or water–alcohol and miniaturized scale emulsion systems (Kim et al., 2003). The sol–gel method has likewise been utilized, yet the presentation of silver was completed from a scattering of a silver salt in the pre-integrated gel (Richter et al., 2004). Like alternate supports, the utilization of this process prompted silver particles of nanometre dimensions, however, with an expansive size distribution. In the condition of additional oxygen (Arve et al., 2006), some of these studies specified that in this procedure the specimen mean molecule size or molecule size dispersion alone could not clarify the extensive contrasts noticed in the catalytic activity (Arve et al., 2006). It was observed that in this procedure, hydrogen had a notable impact on the temperature range over which a NO_x reaction with octane could be decreased through the Semiconductor-Controlled Rectifier SCR (Burch et al., 2004). Further studies, taking into account in-situ Extended X-Ray Absorption Fine Structure EXAFS estimations recommended the impact of hydrogen is a chemical response and not the aftereffect of an adjustment in the structure of the active site (Pârvulescu et al., 2010).

2.2.4. Gold (Au)

It has been stated that the catalytic activity of Au nanoparticles is sensitive to the fabrication strategy and the support material because it relies emphatically on the size and state of the Au nanoparticles (Tsukuda, et al., 2011). Specifically, high reactant action has been stated for the Au particles less than a few nanometres in size in the field of heterogeneous research, as well as in the homogeneous catalysts (Sardar, et al., 2009). Prior studies managing heterogeneous Au catalysts concentrated on the utilization of reducible metal oxides, for example, TiO2 as a substrate for Au. As yet, a few systems, including chemical vapour deposition (Okumura et al., 1998), deposition-precipitation (Veith et al., 2009), and cation adsorption, have been adopted for the Au/TiO2 catalysts fabrication. Among these techniques, deposition-precipitation has been the most commonly utilized process for Au loading, and it includes the utilization of tetrachloroauric acid as an Au precursor (Sanada et al., 2013).

It has been recommended that for Au supported on non-reducible metal oxides, for instance, SiO_2 and Al_2O_3, the gold molecule size is essential; while for Au supported on reducible metal oxides e.g. TiO_2 and CeO_2, the interface acts as a critical role (Zhou, et al., 2008). The theory that just nanoscale Au is needed for activity reflects the low-coordinated Au species in nanoparticles as the active locations, and that the action is not a consequence of the electronic structure of the little Au particles (Valden, Lai & Goodman, 1998). However, many studies report that the turnover frequency (TOF) of the CO oxidation process is identified by the length of the Au/substrate interface and rises with reduction in size of the Au particles (Haruta, 1997). A hypothetical study recommended that there is charge exchange from the reducible oxide support to gold, which advances the reaction. It has likewise been accounted for that oxygen can adsorb on the support and encourage the reaction (Grunwaldt & Baiker, 1999). A supervised structure thin film catalysts, containing a bi-layer Au film supported on TiO_2; was recently demonstrated to be the most efficient construction for CO oxidation, whereas 3-D nanoparticles on Titania were less efficient (Chen, 2004).

Moreover, because of the challenges in controlling the catalyst structure, there is no immediate confirmation demonstrating the site of the active species. The Au surface,

the support surface, or the gold/support interface all have been proposed as substantial factors for activity (Zhou, Kooi, Flytzani-Stephanopoulos & Saltsburg, 2008).

2.2.5. Platinum and ceria (Pt+CeO_2)

Platinum and ceria are two of the crucial components utilized in three-way exhaust systems for the control of fumes emission from vehicles (Heck & Farrauto, 2001). At low pressure, the pure ceria surface demonstrates no room-temperature uptake of either CO or CO_2. Such surfaces are not catalytically-active under special conditions, however, it can lead to massive modification of the surface with the creation of strongly-bound C/O-complexes under high temperatures, and the cerium oxide reveals facile re-oxidation and reduction processes at these advanced pressures (Zarraga-Colina & Nix, 2006).

The preliminary growth of Pt on ceria at room temperature presents a high Pt diffusion. At low loadings there is indication for some Pt oxidation, but at higher loadings the Pt is dominatingly available as crystalline metal. Previous studies of low pressure adsorption on the Pt/ceria model catalysts uncover a quick uptake of CO and easy separation of CO_2 to give mainly adsorbed CO (Zarraga-Colina & Nix, 2006).

It has been discovered that alloying Pt with transition metals, e.g. Ni, Co, Rh, and Fe can successfully lessen the Pt loading by improving both the catalytic activity and consumption of Pt (Zhang et al., 2012). Theoretical and experimental studies have proposed that Pt-based bimetallic catalysts with a thin Pt skin surface are a perfect structures for Oxygen Reduction Reaction ORR because the underneath alloying impact, which causes a modification to d-band centre of Pt surface atoms, can advance the catalysis function (Stamenkovic et al., 2007). De-alloying has been verified to be essentially an efficient method for engineering structures of the core-shell nanoparticles bimetallic catalysts due to the simplicity of removing the less-noble transition metals by a selective etching approach, and producing a Pt passivated surface (Ge et al., 2013).

2.2.6. Magnetic nanoparticles

Magnetic nanoparticles are a group of nanoparticle which can be engineered by applying magnetic fields (Gao, et al., 2010). These sorts of particles commonly involve magnetic components, for example, iron, cobalt or nickel and their composites. Recently, these particles have attracted the attention of many researchers owing to their significant properties which could ensure prospective applications in catalysis, magnetic resonance imaging, biomedicine, data storage, and environmental remediation (Wang, et al., 2010). Among others, gold and silver nanoparticles are receiving massive interesting because of their novel optical properties regarding the surface plasmon resonance (Haes, et al., 2004).

Metallic nanoshells that consist of a concentric noble metal shell and a magnetic core have been involved in numerous uses such as heterogeneous catalysis and in trace analysis. Meanwhile the magnetic particles are easily recovered from a mixture of solution phase without filtering and/or centrifugation. For this reason, $Fe_3O_4/SiO_2/Ag$ nanoparticles in a chemical production can be re-used multiple times by using a neodium magnet (Shin, et al., 2012).

2.2.7. Nickel (Ni)

Nickel-based catalysts are generally utilized as a part of heterogeneous catalysis because of their high hydrogenating traits. Numerous parameters control their catalytic activity in hydrogenation approaches. The activity fundamentally relies on the class of the support which may influence the characteristics of the active phase. The extent of metal–support interface and support acidity appears to show a key role in nickel supported catalyst chemistry (Lin & Vannice, 1993). Silver supported catalysts are considered as a vital catalyst in oxidation and epoxidation reactions (Seyedmonir et al, 1984). Contrary, it is not active in the hydrogenation systems. The rare information stated interestingly demonstrates that silver enhances the stability and the reducibility of the active phase for nickel. The most essential feature for precipitated catalysts is the increase the diffusion and the catalysis function for nickel in silver presence. Consequently, for this reason supported Ag catalysts can remarkably be active toward hydrogen or in the hydrogenation reaction (Wojcieszak, et al., 2008).

2.2.8. Silicon (Si)

Silicon is a multipurpose material having various beneficial properties, for instance, mechanical strength, high thermal conductivity, chemical inertness, and stability. Additionally, silicon micromachining innovation is broadly used and offers the likelihood of incorporating functional components, for example, temperature sensors, heaters, and optical elements (Soltani et al., 2014). Finally, it permits engineering catalyst bed of thin windows which can be probed by diverse spectroscopic approaches. Silicon-based microreactors are currently utilized as a part of a few reactant applications, mainly, in fuel cells, CO oxidation, and gas sensors (Baier, Rochet, Hofmann, Kraut & Grunwaldt, 2015).

Hua et al. (2009) exploited a substrate of silicon nanowires (SiNWs) to grow Ag nanoparticles, due to numerous exclusive properties for SiNWs, such as large surface area-to-volume ratio, simplicity of modification and stability to ambient atmospheric conditions, which could prevent agglomerating of Ag nanoparticles. The resulted Ag-modified SiNWs were used as catalysts in the decay of fluorescein sodium when using sodium borohydride (SB) as a reducing factor. In this method, Ag/Si catalysts presented high activity during the reaction when preventing Ag NPs from agglomerating (Hua et al., 2009).

2.2.9. Cobalt (Co)

Cobalt (Co), as a considerably more ample element in the earth's layer than noble metals, has been intensively investigated due to its cheapness and significantly powerful catalytic properties in numerous vital reactions (Ahmedet al., 2009).

Nevertheless, Co nanoparticles (NPs) are substantially more readier to be oxidized in air as compared to the noble metal materials, and consequently guides to the deactivation and poor recycle stability particularly when two recycle applications require a long interval between them, which completely restrict their functions (Grass, Athanassiou & Stark, 2007). To overcome this issue, traditional strategies are focused on controlling and keeping the catalytic reactions under inert atmosphere conditions (Metin, Mazumder, Özkar & Sun, 2010), or depositing some robust external shells of silica, carbon, or transition-metal oxides on Co NPs. Yet, these strategies undergo from several drawbacks like fairly insufficient catalysts,

because of the occupation of active sites by coating substances, expensive and complex method of catalyst fabrication and application (Yamada, Yano & Fukuzumi, 2012). Accordingly, investigating novel strategies to successfully avoid the deactivation of Co NPs is vastly desirable, but yet it is a substantial challenge.

Recently, Co NPs have shown a growing of interesting by scientists who studying the catalyst's role in hydrogen generation from hydrolysis of ammonia borane AB (NH3BH3) owing to their high activities and low cost (Yan, Zhang, Shioyama & Xu, 2010). Practically, for recycle nanocatalysts, it still a major challenge of their easy oxidative deactivation for a long term of air and water exposure; even though Co NPs are difficult to be oxidized under a reductive atmosphere of the AB aqueous solution. Therefore, for this kind of applications, the catalysts activities are well sustained as high as those of the common catalysts. Finally, a probable remedy to recover the intense activities of reusable nanocatalysts is well refreshing processes after each reaction (Wang, Yan, Wang & Jiang, 2013).

2.3. Conventional Deposition Techniques

Standard methods used in manufacturing nanocatalysts are impregnation (Takenaka, et al., 2003), sol–gel (Luisetto, et al., 2008), mechanical milling (Muñoz, Cervantes, et al., 2007) and co-precipitation (Narkiewicz, et al., 2007). Up to date, mechanochemical synthesis is a familiar method to fabricate innovative nanocomposite materials which refers to the chemical reactions stimulated by high-energy ball milling (HEBM) that can enhance the kinetics of the chemical system (components and results) in powder mixtures at low temperatures. In fact, the nanostructured crystalline in mechanochemical technique will be formed by the structural decomposition of coarser-grained features as a consequence of acute plastic deformation during HEBM. This has become a popular method to make nanocrystalline materials because of its simplicity, the relatively inexpensive equipment and the applicability to essentially all classes of materials (Karimi, et al., 2014).

Basically, configuration of NPs with controlled shape, size and distribution is an essential issue to produce catalysts with better performance. The particle size

influences selectivity and activity of a catalyst during a reaction, thereby, it is necessary to alter these parameters precisely. Moreover, the method of catalyst preparation directly affects its function as well as the construction of the active species with respect to their chemical and electronic states within a device (Coq & Figueras, 2003). Consequently, the control of growth and well- known morphology for the selected samples are the main key points for deposition of high quality film for catalytic applications (Kapaklis, et al., 2006).

Deposition techniques can be classified into two types which are physical and chemical depositions. Table 6 lists some commonly used methods to deposit metals on the substrate.

a) Physical methods involve sputtering (DC and RF reactive magnetron), ion implantation, pulse laser deposition (PLD) and evaporation (thermal and electron beam) deposition; and

b) Chemical approaches include co-precipitation, sol–gel, impregnation, hydrothermal and chemical vapour synthesis (CVS). (Moshfegh, 2009)

The most common deposition methods, which usually employed to create different topographies for many devices, are:

2.1.1. Growth of metal nanocatalysts by magnetron sputtering:

Sputtering is a physical process of material removal from the surface of a target as solid cathode by attacking the cathode using positive ions as the incident beam with adequate energy from an inert gas discharge. Sputtered ions are typically accelerated with enough kinetic energy of several electron-volts to release from the target surface. Most of the works were synthesized by chemical methods due to the simplicity and low cost. The advantages of this technique include a broad extent of metal elements, uniform particles distribution for final metal thin films and high quality and flexibility of various composite films (Moshfegh, 2009).

Magnetron sputter deposition was usually adopted among other PVD techniques due to its simplicity and can be efficiently used for enormous materials, and many factors can be adjusted, e.g. gas pressure, input power and target/substrate distance in terms of controlling the film characteristics. For example, biasing of a substrate would promote the film growth by bombing the plasma ions, which triggers

enhancing the density and lowering the roughness. High peak power signals could also be used aiming to stimulate the sputtered vapour ionization, which could further expand the current film traits (Dutheil, Thomann, Lucas, Brault & Vayer, 2015).

Table 6 shows the most common deposition methods used in the configuration of catalysts (Moshfegh, 2009)

Method	Fabricated materials
DC sputtering	sputtering Fe nanoparticles Au nanoparticles Ni nanoparticles Cu nanoparticles
RF sputtering	Au :VO2 Au : SiO2 Ag : TiO2 Ag : PEO Ru : Al2O3 Ge : SiO2
PLD	Au, Ag, Ni and metal oxide nanoparticles
CVS	Fe nanoparticles Ni nanoparticles Co nanoparticles
Sol-Gel	Cu nanoparticles Ag nanoparticles Au nanoparticles Fe2O3 nanoparticles TiO2 nanoparticles CdO2 nanoparticles Pt nanoparticles SiO2 nanoparticles SnO2 nanoparticles ZnO nanoparticles

2.1.1.1. DC reactive magnetron sputtering

Direct current (DC) magnetron sputtering is applied to conducting materials (Sultana, 2010), and it is one of the most beneficial techniques, giving excellent deposition rates, good control over the structure of the formed films and great uniformity for deposited films on substrates. Interestingly, the film properties, markedly, vary with altering sputtering power (Prathyusha & Reddys', 2014).

2.1.1.2. RF reactive sputtering

For targets of non-conducting material, the positive charge will build up on the material and it will stop sputtering; therefore, radio frequency (RF) sputtering can be utilised. It can be applied for both conducting and non-conducting materials. In this case, magnets are applied to increase the electrons generation that engaged in ionization process and, consequently, the probability of the number of electrons that strike the Argon atoms will boost, thereby, increase the electron pathways leading to significant increase in the ionization efficacy (Sultana, 2010).

2.1.2. Growth of nanometal catalyst by sol–gel technique:

Presently, sol–gel integration of nano-composites comprised of noble metals nanoparticles in titania TiO_2 and silica SiO_2 substrates has grown dramatically (Brinker & Scherer, 1990) due to compounds homogeneity, low processing temperature, chemical purity of the obtained samples as well as the simplicity of preparing nano-sized metal particles with narrow distribution. In addition, the possibility of controlling reduction and oxidization reactions in small concentrations has made the sol-gel technique one of the most advantageous and adaptable methods for oxide film production (Rahman et al., 2006). Furthermore, this method enhances the preparation of nanocomposite materials with remarkable optical properties. Size, distribution and density of deposited particles are varyed as a function of annealing temperature and the operated time (Raffi, Akhter & Hasan, 2006).

2.2. Nanostructures Fabrication Techniques:

Top-down and bottom-up methods are commonly used to manufacture nanostructured devices. As reported in the literature, the top-down procedure employs various lithography approaches to create nanoscale patterns, typically in two-dimension (2D) features. The bottom-up method exploits molecules and colloidal particle interactions to construct discrete nanoscale features in both two and three dimensions (Gates et al., 2005).

2.2.1. Electron Beam Lithography

Electron-beam lithography (EBL) is considered as an effective technique for nano-scale feature fabrication which widely applied to characterize various substances. It is fundamentally applied in micro/ nano electromechanical systems MEMS/ NEMS, and in bioengineering research (Zhang et al., 2005). The uniformity of the e-beam resist covering the surface is a critical requirement for a reliable micro or nanoscale e-beam lithography. Spin-coating resist, typically polymethyl methacrylate PMMA, is the most common method to realize homogeneous coverage layer, however, it fails in the case of non-flat surfaces owing to edge-bead effects (Kelkar et al., 2004).

Additionally, EBL on substrates with trenches or with highly curved surfaces extremely challenging. To overcome these challenges, alternative resist-deposition ways have been developed involving photo resist evaporation (Zhang, Con & Cui, 2014), spray coating, dry-film photoresist (Leech, Wu & Zhu, 2009), or even films of ice (Han, Kuan, Golovchenko & Branton, 2012). The spray coating route is especially suitable for sharp substrate structures like deep trenches if specific spray coating apparatus, and a complex enhanced mixture of PMMA with acetate and ketone to accelerate evaporation during the coating treatment are utilised. Recently, thermal evaporation of polystyrene (PS) has been used in EBL to improve the resolution to 15 nm, but in general, PS has poor exposure sensitivity compared to PMMA and thermal evaporation apparatus makes the process more complex and expensive. While, ice resist has been applied to brittle and non-planar features like carbon nanotubes, this method can be only operated by using particularly designed e-beam lithography and e-beam evaporation systems to control the temperature at levels below 120 K, thus, increasing the cost and restricting the target substrates selection. Interestingly, e-beam lithography on abundantly curved surfaces becomes as easy as on flat surfaces by applying a novel approach innovated by Chang, Zhou, and Zettl in 2014. It involved a dry transferred PMMA film which matches and adheres closely to the curvature of the non-planar design after post-transfer bake, contributing a uniform PMMA coating (Chang, Zhou & Zettl, 2014). The main advantage of this innovation, so far, is its importance in overcoming the light diffraction limit of current optical lithography, which significantly gives fourfold better resolution and lower cost compared to conventional optical lithography. EBL has one key limitation in its utility, which is its low throughput (Yuan, Yu & Pan, 2012)

The technique can also be hampered by several aspects that can affect the EBL resolution as highlighted below:

- Spot size
- The mechanical stability of the resist.
- Secondary-electron range.
- Electron scattering.
- Resist development. (Manfrinato et al., 2013)

Practically, there are two sorts of EBL approaches: variable shaped beam (VSB) and character projection (CP) techniques. In VSB at first, the design is usually divided into a set of rectangles, and each shape would be shot into resist by a sequential dose of electron, as shown in (Figure 1). Thereby, the final processing time of this method boosts with the beam shots number. This considerably influences its throughput to be very low toward the modern complicated manufactures, which is recently composed of a tremendous number of small rectangles. Secondly, the CP technology has been invented to advance the throughput of VSB methods. The major idea is to pattern some complex characters in one electronic beam shot, instead of printing multiple small rectangles. Thus, this substantially leads to reduce the total manufacturing time (Yuan, Yu & Pan, 2012).

The proximity effect correlated exposure in EBL is a result of electrons scattering owing to their collisions with each other and with atoms in the substrate and the resist. This dependent exposure of an unprinted zone, which caused by the exposed Gaussian dose shape. The expanding of the electron beam up to 10 nm is a function of the of the incident resist thickness, the resist material and the acceleration voltage. However, the backward scattering electrons essentially takes place as a result of their interactions with the substrate atoms. Accordingly, the intensity of backscattered electrons depends on the substrate material and the acceleration voltage (Manheller, Trellenkamp, Waser & Karthäuser, 2012).

.

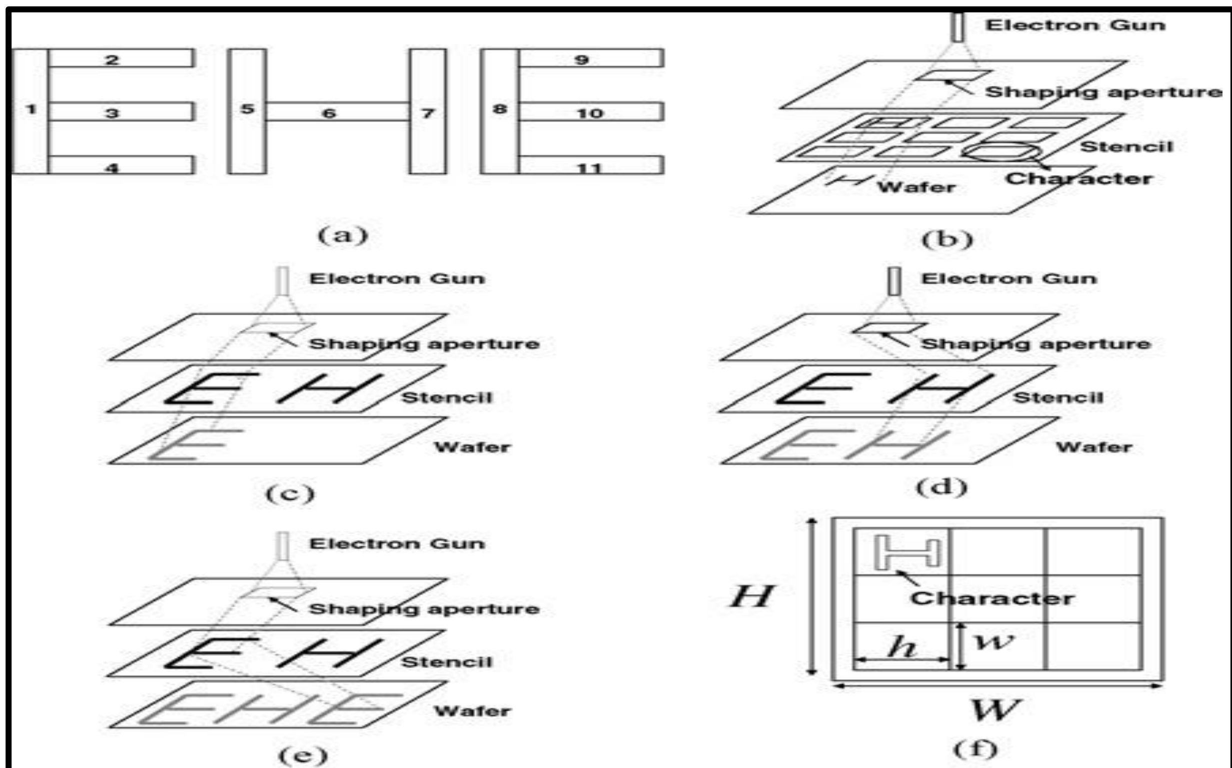

Figure 1 shows the "EHE" pattern was decomposed into 11 rectangles and then required total 11 shots (Yuan, Yu & Pan, 2012)

2.2.2. Nanoimprint Lithography NIL

There has been a growing interest in fabricating nanostructures on curved surfaces and micro-scale objects, especially in applications such as artificial compound eyes, hemispherical electronic eye cameras, photovoltaic devices, image sensor arrays, actuators, and optical fiber sensors (Shen et al., 2013). Though a number of techniques have been proposed for patterning nanostructures on non-planar surfaces, very few attempts have successfully transferred the nanostructures into the matrix of a non-planar substrate. Nanoimprint lithography (NIL) provides large area, high-resolution nanofabrication at low cost and high throughput. New platforms that have been explored for NIL include mask aligners, roll-to-roll imprinting, optical-fiber lengths and optical-fiber-facets (OFF-NIL). To date, OFF-NIL has demonstrated periodic diffraction features with dimensions of 250 nm, and 630 nm, and nanorods for surface-enhanced Raman scattering (SERS) with diameters approximately 110 nm (Kostovski, Chinnasamy, Jayawardhana, Stoddart & Mitchell, 2011).

Nanoimprint lithography commonly uses inflexible flat molds under mechanical load, and is incompatible with the imprint process on curved and non-flat surfaces (Chou, Krauss & Renstrom, 1996). A set of techniques known Soft lithography has been adopted to fabricate microstructures devices by using an elastomeric pattern transfer element mechanism (Xia & Whitesides, 1998). This technique can be applied for microsprings, microtransformers, and long-period gratings on spherical surfaces and cylindrical platforms. However, soft lithography which basically employed for sub-100 nm systems depends on commercial elastomeric substances of low elastic modulus (Huang et al., 2005). The lack of a trusted data is another barrier can be a considerable hurdle in creation nanostructures on arbitrary non-planar surfaces (Black, Paul, Aizenberg & Whitesides, 1999).

To date, numerous coating methods have been presented for the disposition of a resist layer on a substrate. One of the common and widely used methods is spin coating which capable of yielding high film thickness uniformity in addition to short coating time. In the case of non-planar, curved and rough substrates, the physical topology restricts the fluid flow which is driven by centrifugal force. Nonplanar substrates prevent the coating process from being effective, leading to resist thickness variation, called striation (Martinez-Duarte et al., 2010). Spray coating and its imitative routes such as dispensing and nano-spraying, as compared with spin coating, are the most reliable techniques to deposit resist on arbitrarily shaped and sized samples, as well as three-dimensional structures. Additionally, spray coating consumes extremely small amounts of resist than for spin coating, due to no spin off resist waste. In contrast, it is a challenge to produce a uniform resist film with sub-micron thickness, and this requires expensive equipment and particular resist solutions (Liang, Tan, Fu & Chou, 2007). Similarly, dip coating, which is appropriate for arbitrarily shaped and bulk structures, produces inadequate film uniformity (Yimsiri & Mackley, 2006). Electro-coating of photoresist is a desirable method for 3D interconnects and chips stacks, providing a conductive layer (Zhang, Luo & Liu, 2013). To sum up, only few available methods for resist film deposition would provide sufficient and uniform thin resist layers on non-planar and sub-micron sized substrates.

In terms of NIL resist processing, there are two fundamental types of the process: thermal NIL and ultraviolet (UV) NIL. Thermal NIL, known as hot embossing, is the first type of NIL proposed by Chou and his team in1995. It involves imprinting onto a resist of thermally tempered thermoplastic polymer (Chou, Krauss & Renstrom, 1995). The standard thermal NIL process uses from a mold that is heated up to a boosted temperature greater than the glass transition temperature (Tg) of the polymer resist. When the hot mold contacts the resist, the resist will be warmed up and become soft in its molten phase. Thereby, it will fill in the mold pits under an appropriate imprinting time and pressure. The increase of temperature is essential since the yield strength and elastic modulus of the resin (polymer) decrease considerably when the temperature became larger than T_g. However, temperatures much higher than Tg can trigger crucial damage to the resist film. Then, the imprint temperature will be dropped below the Tg of the resist to keep it in the solid phase before lifting the mold. Accordingly, the patterns/structures are transferred from the mold to the resist (Kooy, Mohamed, Pin & Guan, 2014).

In contrast to the aforementioned NIL process, UV NIL involves stamping into a resist layer comprised of a liquid photopolymer, followed by curing via UV exposure. This exposure solidifies the resist due to cross-linking in the polymer (Colburn et al., 1999). The subsequent steps of the imprint process are similar to the hot embossing process. For further explanation, a comparison between standard UV NIL and thermal NIL processes is shown in (Figure 2).

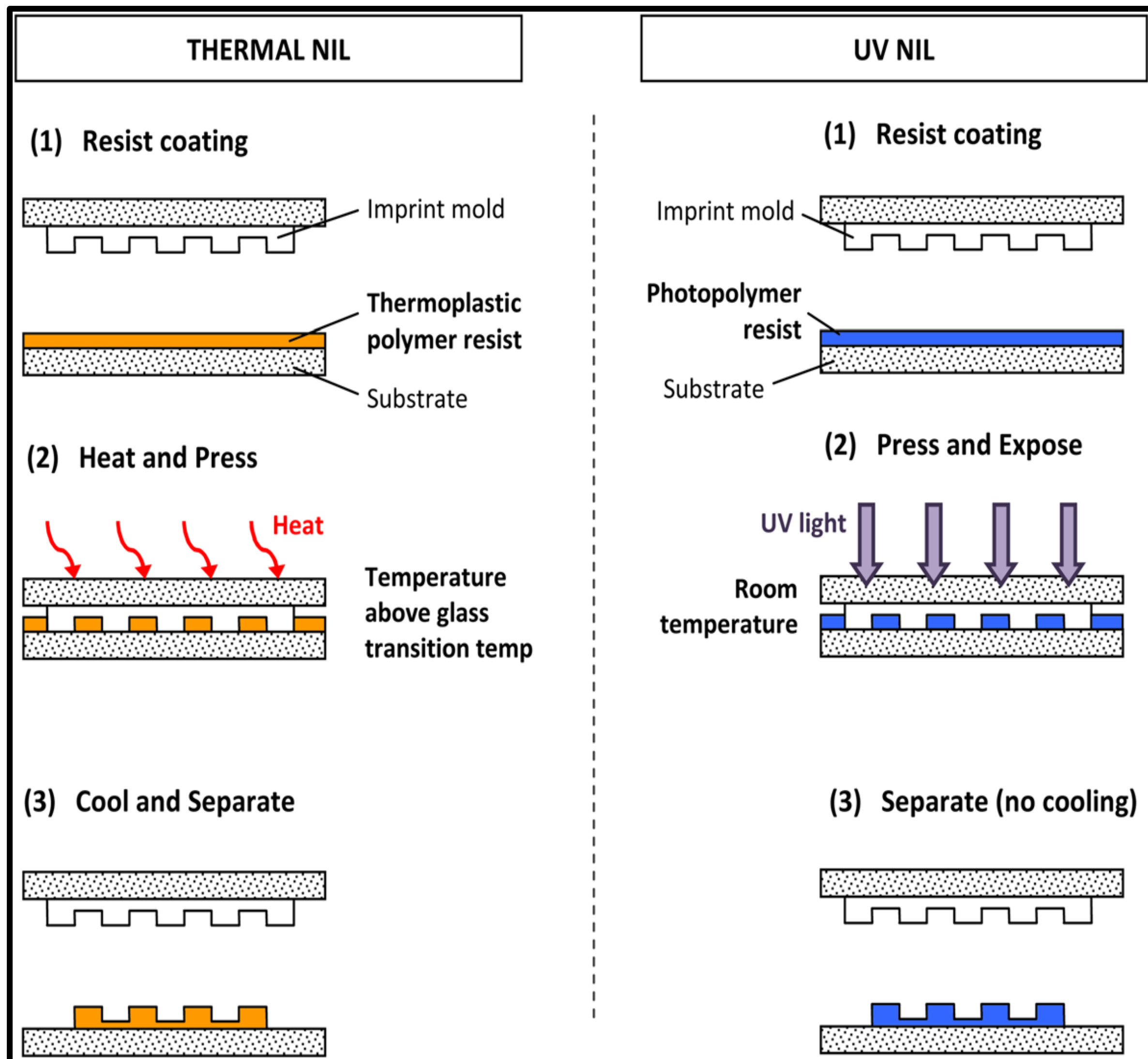

Figure 1shows a comparison between standard UV NIL and thermal NIL processes

(Kooy, Mohamed, Pin & Guan, 2014)

The UV NIL process has numerous prominent benefits over hot embossing NIL. This includes the ability of UV NIL to be performed at room temperature, which helps eliminating the problems would be resulting from thermal expansion deviations among the mold, resist, and substrate. Additionally, the imprinting method operates with less viscous photoresists and can be performed at a lower imprint pressures than thermal NIL processes. The low viscosity of the resist also permits resist to occupy the mold pits in a short time, whereas the elimination of the temperature cycle enhances the process throughput (Kooy, Mohamed, Pin & Guan, 2014).

2.2.3. Substrate Conformal Imprint Lithography SCIL

In Nano Imprint Lithography (NIL) a rigid stamp is pressed into a resist film, which can be treated thermally or by exposing to UV radiation. In this way, so miniaturised details can simply be replicated. However, hard stamp lithography techniques are very sensitive to even tiny contaminants which may prevent a perfect contact between the stamp and the resist interface over large areas. There can also be issues in releasing the stamp from the cured resist with damage the resist layer or pattern deformation resulting. This is a non-trivial issue (van Delft, et al., 2010). On the other hand, soft stamp lithography techniques imply a different methods of stamp removal such as sagging and pairing (Xia & Whitesides, 1998).

Consequently, Substrate Conformal Imprint Lithography (SCIL) has recently developed by Philips Research. It is a replication technology in which a flexible nano-imprinting can be performed even in the presence of defects. It utilizes stamps with a high modulus pattern layer of polydimethylsiloxane (PDMS) attached onto a glass sheet with a low modulus intermediate layer of PDMS. This stamp sheet is fixed on a channel-structured vacuum plate. Then, applying sequential pressure and evacuation to the channels (grooves) to control the contact between the stamp and the resist layer followed by careful release after UV curing (Ferry et al., 2009)

Common resists for SCIL use inorganic compounds employed as etch masks for substrates such as Si, SiO_2, GaN or metals. Their chemical content makes them suitabile for etching process. Furthermore, all conventional resists for SCIL require extensive curing times (3–15 min) (Ji et al., 2010). Fader et al. investigated pure organic materials to produce a suitable imprint resist for etch masks for various substrates with the advantage of decreasing the curing time relative to inorganic resists. Adoption of UV curing polymers essentially reduces the total time for SCIL process by 50% in total (Fader et al., 2012).

SCIL technology has multiple ***advantages*** over other rigid stamps methods.

- Ideal contact can be made over large areaswithout the aid of a high pressure as the substrate is completely covered by the flexible stamp (Verschuuren, 2010).

- Micro scale air inclusions and partially filled structures are prevented because silicone rubber has great permeability for gasses and solvents which permits the air to penetrate into the stamp (Verschuuren, 2010).
- Particle contaminants are not so important an issue as the rubber can locally deform around a particle avoiding any destruction to the stamp or substrate (Verschuuren, 2010).
- Separation of a rubber stamp from a rigid imprinted sample is mainly followed be temporary deformation of the rubber after release. Consequently, this avoids any potential damage to patterns in the resist or stamp. This enables the reproduction of features with a high aspect ratio compared to (UV-NIL) where the aspect ratio is often restricted to below 1.5 (Verschuuren, 2010).
- PDMS has a naturally low surface energy and is chemically inert, so an anti-sticking layer to prevent adhesion between stamp and substrate is not always required (Verschuuren, 2010).

2.3. Etching Process

Etching is the process of using strong acids or harsh chemicals to etch cut into the exposed parts of a material surface to form various structures shapes and sizes in samples of interest. Etching techniques are generally classified into two categories: wet and dry etching.

2.3.1. Wet etching

In this method, the etchant is provided from the liquid phase and can be carried out in a vessel like a beaker (Li, 2012). The major principle of the wet etch methods is the oxidation of metal by special oxidising agents followed by configuration of metal-ligand complexes to detach the oxidised metal from the surface. Therefore, wet etch rates depend on the solubility of ligand complexes and the chemical ability of metals to react with oxygen (Choi & Hess, 2014).

Wet chemical micromachining technology is commonly exploited in MEMS industry for its high rate of etching and selectivity. Nevertheless, there is one negative aspect in terms of mask . Masks are also etched during the etching process. Thus, it was proposed by Ojur and his colleagues in 2013 to innovate a mask that is either

unaffected or dissolves slower than the exposed substrate. In wet etching, etch rates and selectivity can be controlled by in different ways:

(a) Altering crystallographic planes of the substrate.

(b) Regulating temperature of the etching solution.

(c) Chemical composition of etchant solution.

(d) Concentration of dopants in the substrate (Ojur, Ahmad & Haris, 2013)

In bulk micromachining, Chemical wet etching is also classified into further two subdivisions: isotropic and anisotropic. Firstly, isotropic wet etching is where the etch rate is not altered by crystallographic direction of the substrate and etching proceeds in all directions at uniform rates as shown in (Fig3a). Secondly, anisotropic wet etching where the etch rate changes with crystallographic orientation of the substrate as shown in (Fig3b). To control etching process and to obtain uniform etch depths through the wafer, etch stops techniques are usually used.

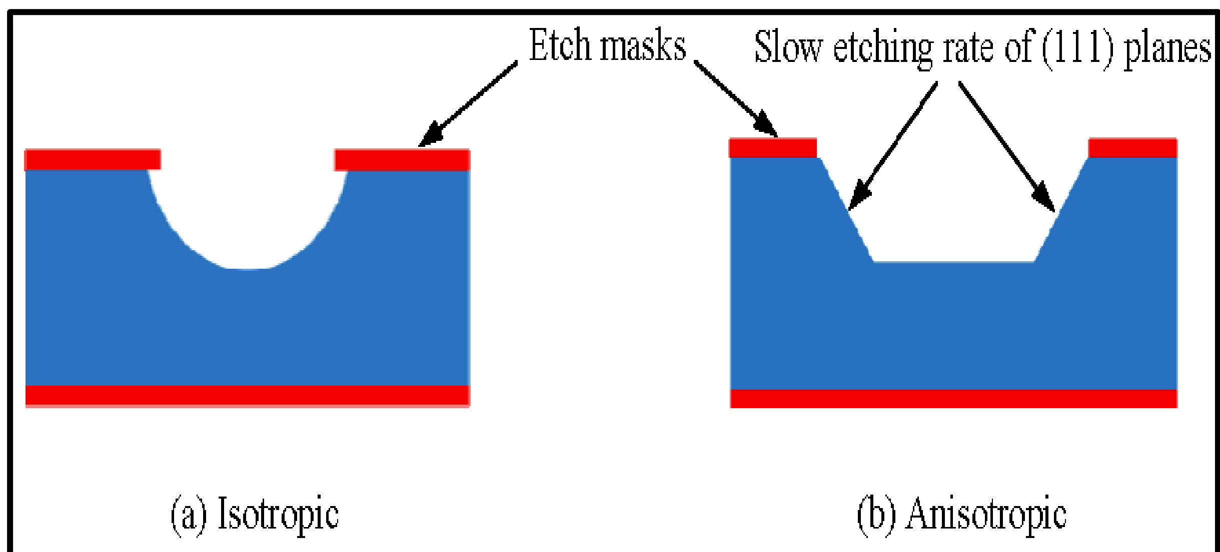

Figure 2 shows difference between (a) isotropic and (b) anisotropic wet etching

(Ojur, Ahmad & Haris, 2013)

2.3.2. Dry Etching

In case of dry etching; the vapour phase is the source of etchants. Conventional dry etching techniques embrace chemical assisted ion beam etching (CAIBE), reactive ion etching (RIE) and inductively coupled plasma (ICP). All of these methods require plasma generation, vacuum and ion optics conditions (Li, 2012).

The basic principle of plasma etching refers primarily to the reaction between unbiased gas radicals and the material surface to create volatile etch products which are then desorbed from the surface.[32] Many metal halides used in plasma etching processed are volatile such as TaF_5, WF_6, $AlCl_3$ CrO_2Cl_2 or (Tang & Hess, 1984). Conversely, other metals such as Cu, Au, and Ag do not form volatile products in standard halogen-based plasmas (Kuo & Lee, 2001). Therefore, unconventional methods have been harnessed to support etch product removal; these methods involve elevated temperature, enhancement of the energy of ion bombardment, photon exposure and finally wet etching to separate product species (Li, 2012).

By choosing a suitable mask to avoid local etching, both wet and dry processes are extensively able to create 3D features with topographical variations that are determined by the mask and etching circumstance. Most semiconductors are fabricated by isotropic wet etching approach, in other words, etching continues uniformly in vertical and horizontal directions. This leads to loss the lateral resolution as related to the mask dimensions by a factor of double the depth, in consequence, not appropriate for manufacturing high aspect ratio structures. Li (2012) stated that there is an exception when adopting a crystal orientation dependent etch rate to facilitate anisotropic wet etching which produces bounded structures with noticeably slow etch planes (Li, 2012).

Dry etch conversely, can be directional since etchant has the ability to be ionised in the gaseous media and accelerated towards the chamber surface during the etching process. Additionally, high aspect ratio structures can be designed by applying numerous methods, for instance, the Bosch or so-called deep RIE etching and cryogenic techniques. In fact, the lateral resolution is delimited by the mask characteristics. Whereas, the attainable depth is restricted by specific effects such as bottling where the trench base pinched off, and also aspect ratio dependent etch rate

where the etch rate decreases considerably with increasing the aspect ratio or the depth (Wu, Kumar & Pamarthy, 2010).

There are couple of undesirable side effects with dry etching method. Sidewall roughness of the etched patterns, particularly, the scalloping effect correlated to Bosch time multiplexed passivation, and ion induced damage to the trench sidewalls which triggers a significant increase in surface states that causes degradation and nonradiative recombination of carrier mobility (Li, 2012).

2.4. Lift-Off Finishing Method

It is a common fabrication way often used in outlining nanoscale structures in micro/nanofabrication processes (Liang, Kohsaka, Matsuo, Li & Ueda, 2008). The lift-off refers to an additive process that requires a sacrificial layer of special substances to behave as a temporary mask. After imprinting the desired patterns by utilising one of diverse lithography techniques, the whole sample surface, which contains the patterns on both of the wafer and the sacrificial layer, is coated by the target material via deposition. The next step is applying the sample to a chemical solvent to develop the sacrificial layer and consequently the deposited material on the top of this layer is lifted off as this layer is washed off (dissolved) but the deposited material on the identified structures remains because it is stuck on the substrate surface (Maraghechi, Cadien & Elezzabi, 2011).

However, the widely used lift-off process presents a low yield and undesirable rough edges of fabricated nanoscale structures which called overhangs or rabbit-ear-shaped (Hwang, Jung, Jeong & Lee, 2009). There are two major causes lead to breakdown the current lift-off process. Either because of the contaminations that are not well-removed from the exposed surface prior to deposition or the deposited material has weak adhesion forces to the substrate due to its chemistry and surface conditions (Maraghechi, Cadien & Elezzabi, 2011).

2.5. Damascene lift-off process

A novel technique has been investigated by Maraghechi and his coresearchers in 2011 to solve the essential problems faced the conventional lift-off technique which called damascene lift-off process. Prior to the deposition of the chosen material, it is preferred to use an etching process to keep the developed area of the exposed surface simultaneously clean and rough to enhance the adhesion of deposited material, and consequently a high yield process is achieved. Moreover, in the current damascene lift-off process, the line-edge roughness of the material deposited is reduced, whilst the resist thickness does not restrict the thickness of the deposited material. Recently, very reliable lift-off attempts have been accomplished in which the thickness of the resist was half the thickness of the deposited material (Maraghechi, Cadien & Elezzabi, 2011).

Furthermore, traditional lift-off processes last long time to dissolve the resist by the solvent and then to remove the unrequired deposited material, while the present process has reduced the total time taken to a few minutes. This offers high accompanied yield by a considerable reduction in the process costs and time (Maraghechi, Cadien & Elezzabi, 2011).

2.6. Conclusion

To sum up, PVD and CVD techniques with some common metal catalysts which fabricated by various methods such deposition, impregnation and embedded approaches have been detailed in this chapter. The effect of nanoscience to nanotechnology has evidenced through brief illustration to some imprinting techniques to create nanoscale features such as EBL, NIL and SCIL. Importantly, EBL and SCIL are both of interest in this research. Additionally, etching and lift-off methods which are utilised in in outlining nanoscale patterns have highlighted at the end of this chapter.

Chapter 3

Manufacturing Of Nanostructured Ag-Dots using EBL

3.1. Introduction

Nanoelectronics and nanophotonics are evolving fields that deal with nanoscaled features with dimensions less than 100 nm to enhance extra combination of nanodevices with adapted functionalities. Innovative techniques are engaged for the direct lithography to integrate nanoscaled devices on wafers such as extreme UV lithography (EUV), nanoimprint lithography (NIL), or e-beam lithography (EBL). Interestingly, EBL is the important approach for top-down manufacturing technique exploited for various applications owing to its ability to imprint arbitrary patterns close to 5 nm in scales (Manfrinato et al., 2014).

In this chapter, two main methods used to fabricate Ag dots which are wet etching and lift-off approaches will be demonstrate in this chapter, also. Herein, it is worth mentioning that this study is a unique investigation in field of Ag/SiO_2 in terms of synthesis and fabrication methods. By surfing into various scientific papers and research studies, there are massive investigations in terms of sol-gel method, which depends on dissolving silver compounds with other solvents and then added to SiO_2 into complex preparation procedures, to produce Ag nanoparticles AgNPs containing silica of irregular arrangement around the entire sample (Raffi, Akhter & Hasan, 2006). Other studies deal with incipient impregnation method to synthesise AgNPs with SiO_2 or alloying with other metals like nickel Ni to create bimetallic nanocomposite materials for catalytic activity improvement (Wojcieszak, Monteverdi, Ghanbaja & Bettahar, 2008). Further papers focus on embedding silver with polymers or magnetic metals like iron to be used in reusable catalysts or for biomedical purposes (Hariprasad & Radhakrishnan, 2010) and (Shin, Choi, Park, Jang & Kim, 2009). Therefore, most analysis and comparisons in this thesis are compared with Ag/Si research studies due to the fact that Si substrates naturally compose of a thin layer of native oxide.

3.2. Materials and methods

(1) A SiO_2 wafer was initially cut into many slices of about 1 cm x 1.5 cm rectangles to be cleaned and prepared for silver deposition. The samples were washed with acetone $(CH3)_2CO$ and then isopropanol IPA $(CH3)_2CHOH$ to remove any remaining residuals of metal or contaminants that could exist on the samples surfaces, and then dried with nitrogen.

A deposition process was accomplished by applying physical vapour deposition model Kurt J Lesker PVD75 sputtering system. Firstly, some samples were selected for deposition stage where they well fixed on a special holder coated with gold which usually used in such systems. The samples were stuck by utilising two-side tape of high adhesion ability to keep samples safe and stable within the main chamber under vacuum conditions along the operation time.

A silver target of purity 99.99% was placed in one of the three guns which the chamber was provided with. Next, the holder with the samples was located away over the target; oppositely, or in other words, the samples face the target. After finishing this step, vacuum condition was digitally operated and controlled to achieve pressure rate of 10^{-5}mTorr. The process of pumping pressure down lasted 2h roughly. At the end, the sputtering DC magnetron was supplied to start deposition by evaporation silver atoms from the surface of the target toward the samples to be covered by a uniform thin film. The deposition process was finished by 2-3 min to finally prepare an about 10nm film thickness of Ag on SiO_2 substrate. The sputtering conditions were applied shown in table 7.

Table 7 shows the conditions of depositing 10 nm silver layer

Source	Vacuum pressure (Torr)	Ar flow rate	O2 flow rate	Power W	Deposition rate A°/s	Stabilisation time (min)	Film thickness (nm)
DC	1.79E-3	30	0	50	0.5	2-3	10

This table shows that direct current DC is the supplied bias for sputtering magnetron during the experiment. The deposition process was completed under a pressure of 1.79E-3Torr for (2-3) min with the absence of oxygen to inhibit the growth of silver oxide.

Next, the samples were taken out to start the lithography stage. One sample was chosen for this step and coated with a thin layer of negative photoresist called nLOF2070 diluted in EBR (edge bead remover) as a mixture rate of 1:3, respectively. Spin coating profile was done by using WS-650MZ-8NPP/A1/AR1 model at rotating speed of 3000rpm and acceleration of 1000rpm/s for 45s. The obtained sample was heated up to 100˚C for 1min to ensure good contact interface between the resist and the surface of Ag metal. Then, the coated sample was loaded into Raith e-LINE electron beam lithography system with a current of 0.016ns to imprint desired features. A selective alignment of nanodots was proposed to examine the effect of various doses factors on the uniformity and selectivity of resulted dots.

Four main location references (A) were patterned on the silver film to ease exploring the produced nanodots features of variable dose factors 1, 2, 3 and 4 times with respect to the base dose which was 0.001pC. Figure 7 displays one of these patterns of 1 dose factor exposure as an example for another three.

Each main location reference was followed by four sub-squares which also differed from each other by dose factor value. The top two patterns (a) in (Figure 4) also refer to location references which ease finding the dots of interested under SEM or the optical microscope. Each feature of the four squares (b, c, d, e) includes 100x100 dots arranged horizontally into diverse spacing, 50, 100, 150 and 200 nm, as well as a different exposure dose with respect to the reference dose as 1, 3, 8 and 12 times, respectively (Figure 3).

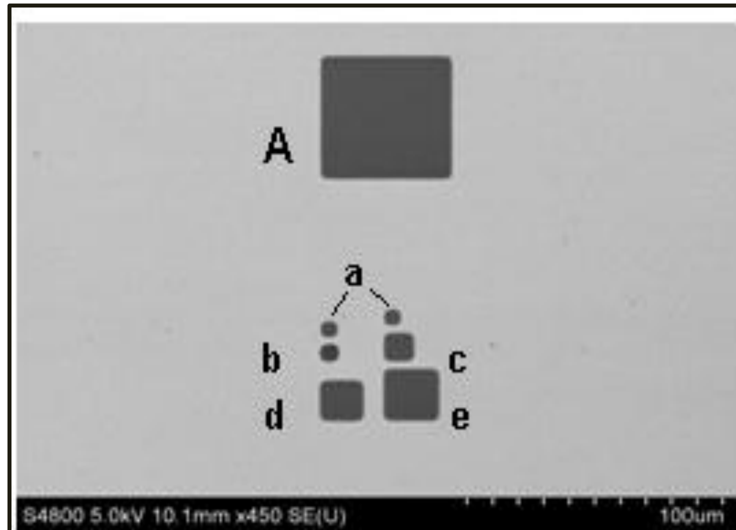

Figure 3 shows one of the standard patterns designed especially for this experiment

The next step was the resist developing by using a specific solution which named AZ726 MIF developer. Different concentrations of developer with water were prepared. 2:1, 1:1, 1:2, 1:3 volumes of AZ726:H2O which should be used in order to ensure a successful developing process. First, the sample was warmed up to 110˚C for 1 min and then rinsed into the first solution of 2:1 for 15 s, then a quick rinse into the other solutions and finally washed into DI water to remove any potential residuals. This process occurred under the room temperature. Because of using a negative photo resist, the only exposed area was remained after resist developing step.

Scanning electron microscopy SEM was the next step to study the morphology of the final surface after developing. The selected sample was loaded into SEM (HITACHI S-4800) and many images were obtained from various places on the investigated surface.

(2) The second attempt was implemented to overcome the problem which happened previously. In this case, a SiO2 sample without Ag layer was utilised to examine the effect of thickness on creating nanodots with optimal consistency and stability where the oxide layer was estimated to be some microns. Same cleaning steps were followed as the last sample, and then patterned by using the same equipment of e-

Line Raith lithography with completely same features that explained in Figure 4. The results were very good when analysed by SEM.

(3) Consequently, the recent results were encouraging to start a new silver deposition with thicker layer. By follow the same steps, as previously, to clean the prepared substrates of SiO_2, PVD sputtering deposition also applied to provide a desired thickness of Ag layer. Slightly different conditions were run in the system to get thicker film of 20 nm silver metal. Table 8 shows how the changing in the power provided affected the deposition rate, which led to increase Ag film thickness.

Table 8 shows the conditions of depositing 20 nm silver layer

Source	Vacuum pressure (Torr)	Ar flow rate	O2 flow rate	Power W	Deposition rate A˚/s	Stabilisation time (min)	Film thickness (nm)
DC	1.82E-3	30	0	120	10	1	20

Then, the sample was located in the EBL system to form the same patterns as recently with little change in exposure dose where it was reduced to factor 10 to become 0.0001pC as compared to previous dose which was 0.001pC.

The previous step was followed by the resist developing process and SEM investigation. The final film appearance was significantly polycrystalline with clear features of silver nanodots. A wet etch approach was adopted because it was more appropriate and easier way than dry etch, especially, for silver etching. From websites of silver wet etching like http://www.cleanroom.byu.edu/wet_etch.phtml, the best rate of etching was expected by exploiting strong acids together with water according to following volumes 3:3:23:1 of H3PO4: HNO3: CH3COOH: H2O, respectively, to give a rate of etching around 10min/100A or 1min/ 1nm which is slow enough to be controlled. The solution was mixed carefully by pouring 1ml of DI water into a large beaker and then adding 3ml of H3PO4 firstly, and next, pouring 3ml of HNO3 carefully; finally 23ml of CH3COOH was added slowly. After preparing the mixture, the chosen sample was immersed into the container of the acidic solution with slow shaking to activate the etch process. The result was unexpected because

of the high activity of the solution which led to fast and uncontrolled rate of etching. Thereby, there is a demand to dilute the acidic mixture to half its concentration by adding extra 30ml of DI water. The obtained etchant solution was adequately suitable to etch a very thin silver film, but still gives a not uniform rate of etching, particularly after aging or leaving the solution for a while.

(4) To improve the research and find out a better way of imprinting silver nanodots with more uniformity and selectivity, a lift-off technique was implanted into two different endeavours. The first was accomplished by coating the required sample with a thick resist layer of PMMA, and the second way was done by using a thin PMMA resist coating.

(A) Thick PMMA resist: C4%

By following the same steps for preparing samples of SiO2 and cleaning them as same as previously, a sacrificial layer of 950PMMA photoresist, i.e. its molecular weight is 950 kilo Daltons, was deposited on a sample surface by a spin coating system (WS-650MZ-8NPP/A1/AR1 model). The resist was composed of 4% PMMA diluted with Chlorobenzene solvent C6H5Cl. The coating conditions were set as 500rpm for rotation speed and acceleration value of 500rpm/s for 5s of spin duration. The thickness of the produced layer was about several thousands of angstrom according to the literature (Figure 5). Next, the coated sample was positioned on a hot plate at high temperature of 180˚C for 1min, and then loaded into Raith e-Line system to be exposed to an electron beam radiation. In this experiment, a different pattern was imprinted to provide a wide range of doses varieties on one sample. The proposed features were arranged in an array of 20 standard patterns shown in (Figure4). Each pattern was imprinted with various dose exposures than the others with respect to base dose which was 0.001pC. The array features were exposed to 1, 2, 3,…., 20 dose factor, separately (Figure 6).

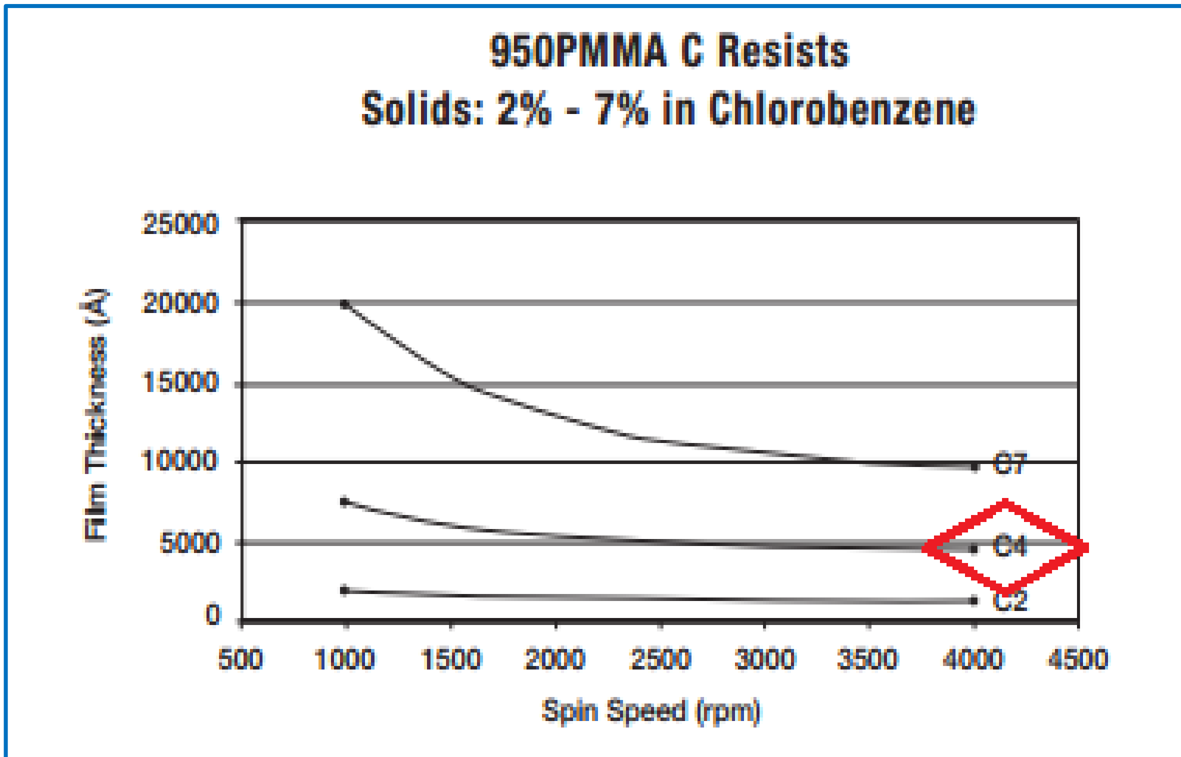

Figure 4 displays the spin speed versus film thickness curve

http://microchem.com/pdf/PMMA_Data_Sheet.pdf

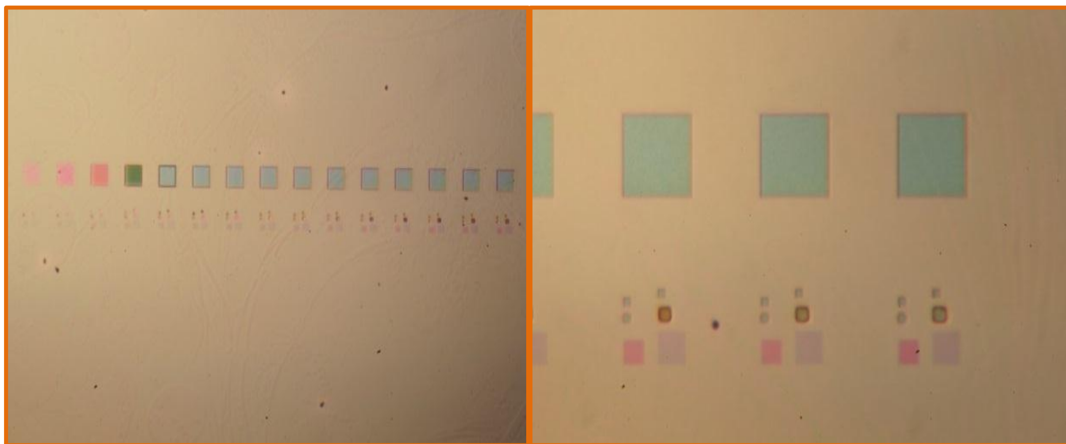

Figure 5 present the array features onto thick PMMA layer

Thus, the exposed photoresist was ready to be developed by a suitable developer. To terminate this process and prevent scum generating, PMMA was immersed into 1:3 volumes of Methyl isobutyl ketone (MIBK): Isopropyl alcohol (IPA) for 30s and

immediately washed with IPA to remove any unacceptable residuals followed by N2 blow dried.

Because of PMMA is a positive photoresist, the exposed areas were removed after curing with the developer. Therefore, the sample became ready to deposit the target metal (Ag) onto whole surface. The same circumstances that set for 20nm silver deposition were also applied in this part. The next step was removing the remained PMMA by lift off process by rinsing the final product (SiO2+Ag+PMMA) into acetone solvent. The SEM images of the surface morphology were disappointing because the lift off process, not removed, only the resist, but also the metal and consequently the imprinted features.

(B) Diluted PMMA resist: C1%

To complete this study successfully, another approach was investigated. Because of the drawbacks that occurred with thick PMMA sacrificial layer, a thin photoresist was prepared from 950PMMA diluted with Chlobenzene solvent. The same steps of cleaning and coatig samples were pursued similarly to preceding process with major differences in the spin caoting operation cinditions. The spin rotating speed was increased to 4000rpm, the system accelaration was 1000rpm/s and the caoting duration was 45s to produce a very thin stencil layer of C1% PMMA of thickness few thousands of nanometers. Then, loading the sample into e-Line apparatus to create features of dots array arranged into two rows of 20 standard patterns each. The main dose value for the both rows was 0.0001pC but each feature differ from the others by its dose factor. Or in other words, the dose factor in the top row were 1, 2, 3,…., 20, whereas in the bottom row features were set into 2, 4, 6, …., 40 times the base dose (Figure 7).

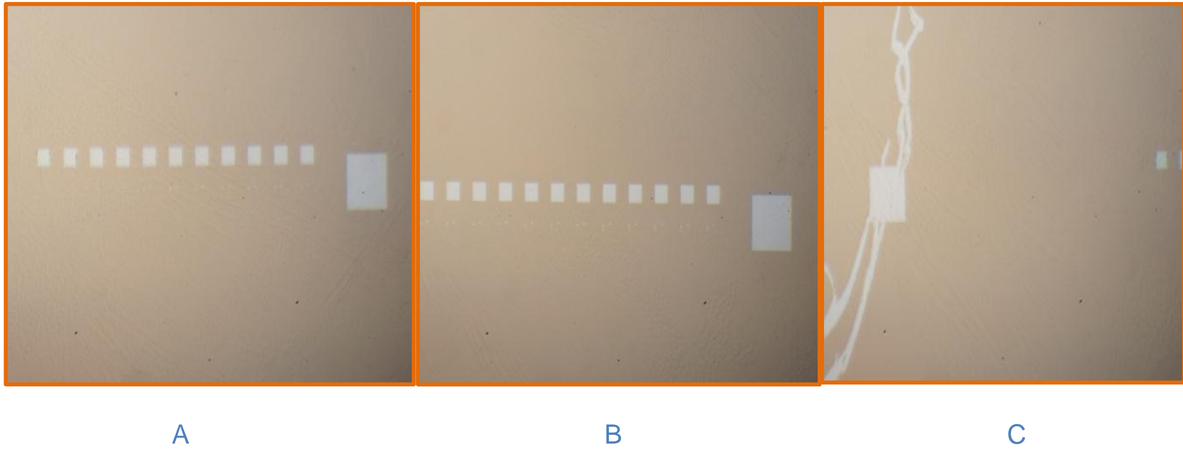

A B C

Figure 6 shows the two rows of dots array imprinted onto C1%PMMA

Figure 7 (A, B) display the sample after developing with 1:3 volumes of MIBK:IPA. The patterns appear to some extent clean from residuals as shown in (Figure 7C) where the white colour refers to the sample surface below the resist film. The following step was deposition a silver thin film by the PVD sputtering magnetron device. The operating conditions were similar to 20nm Ag film deposition. After that, acetone was used to lift off the metal and the remained resist.

3.3. Results and Discussion

This part of the present study focussed on deposition silver thin films by various conditions and thicknesses to obtain the optimal morphology required to pattern nanodots features as a preliminary research for nanocatalysts application in the future.

Firstly, for 10nm Ag film thickness, the images gathered from the SEM showed irregular surface and failed imprinted pattern with a major appearance of islands topography. Figure 8A presents the discontinuous Ag thin film before etching with islands of SiO2 surface underneath, and some small grains with different shapes are distributed randomly. As a result, the features appearance was clearly meaningless (Figure 8B). It is a challenge to deposit a continuous silver thin film below 10nm. Sanjay et al. stated that an Ag thin film with thickness (~5nm) was deposited on a polished Si substrate using the electro-less metal deposition process at room

temperature resulted in a thin layer of Ag nano-islands consistently covered the entire sample surface (Srivastava et al., 2012). For this reason, the EBL process was not successful to produce patterns of uniform and clear nanodots.

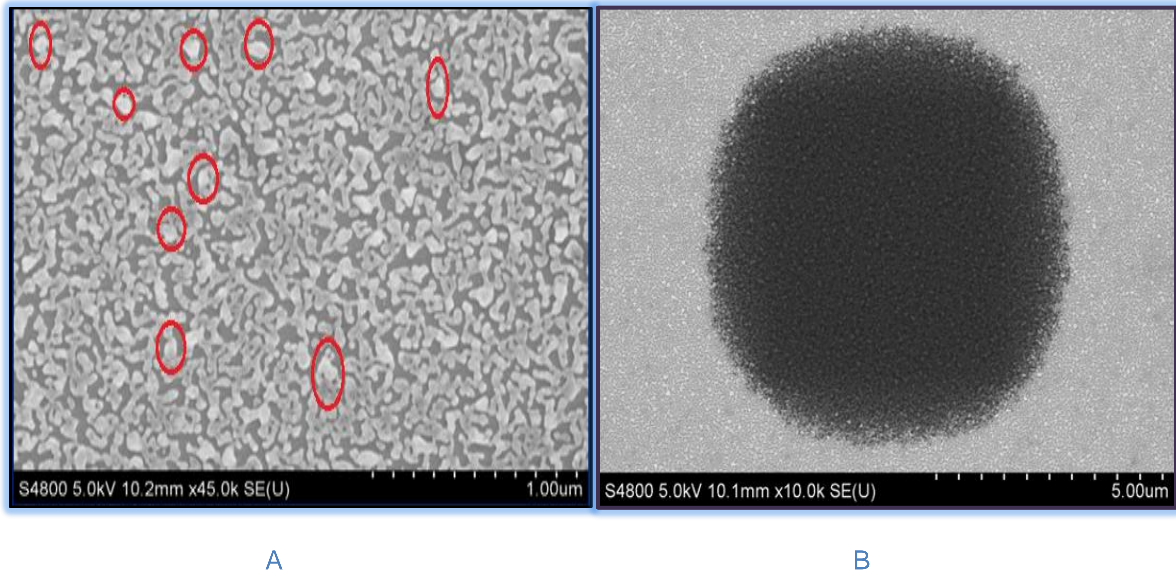

Figure 7 SEM scan displays the 10nm Ag thin film with A) some grains of random size and shape, and B) unclear features

Several authors have reported that the morphology of Ag thin films influence by the film thickness and the preparation method (Rakocevic, Petrovic & Strbac, 2008). As mentioned before, the deposition process was conducted by DC sputtering magnetron which gave the island appearance for 10nm Ag film thickness. While, depositing silver on a highly polished glass substrate by RF sputtering magnetron for the same thickness produced grains of hexagonal shape crystals with sizes of (200–250)nm which slightly decline with increasing the rate of deposition with disappearing of the grains of hexagonal shape (Rakocevic, Petrovic & Strbac, 2008). As stated in literature, the film morphology can also affect by various parameters, such as the deposition time, the sputtering power and also the gas ions used for vacuum (Xiong et al., 2000), substrates temperature and material (Mashaiekhy, Shafieizadeh & Nahidi, 2012), the sputtering pressure and substrate texture orientation (Kapaklis, Poulopoulos, Karoutsos, Manouras & Politis, 2006). For example, by increasing the sputtering power or time deposition, the grain sizes significantly increase (Xiong et al., 2000). For later deposition method of 20nm Ag film, the effect of film thickness and the power of sputtering system will be elucidated in terms of its morphology.

It obviously evidenced by Dutheil, et al. that depositing Ag onto Si wafer of extremely thin layer of native oxide resulted in a continuous thin silver film of thickness less than 11nm at room temperature. This behaviour considered to be related to capability of silver to wet Si wafer (Dutheil, Thomann, Lecas, Brault & Vayer, 2015).Hence, in the present research, Ag metal deposited onto a thick oxide layer which grown thermally provided a non-continuous film. This observation could be explained either by the fact of low chemical affinity (-8) between silver and oxygen which could cause the aggregation of silver atoms randomly to form irregular islands shape, or because of the sputtering pressure for argon ions was too low (1.79E-3 Torr ~ 0.24Pa) where the optimising value is 2.5Pa (Dutheil, Thomann, Lecas, Brault & Vayer, 2015).

To evolve the results, an attempt was implemented on SiO2 samples to improve the quality of imprinting dots. As presented before, the Ag film deposited was very thin (10nm) where the oxide layer of SiO2 estimated to be several nanometers. The results were completely in agreement with what expected. Figure 9(A, B &C) displays the uniformity and high quality dots imprinting with thick oxide layer, and also shows different spacing distances for three different patterns of dissimilar doses.

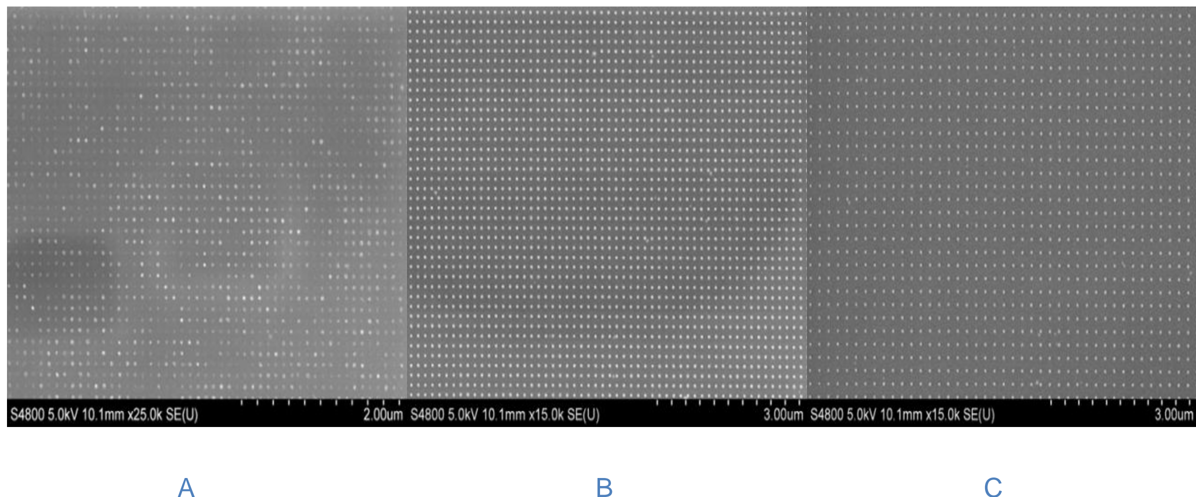

A B C

Figure 8 SEM scan shows dots patterns onto SiO2 surface: A) 100nm spacing of 6 time main dose. B) 150nm spacing of 16 times main does. C) 200nm spacing of 24 times main dose. (100 nm spacing) x6 base dose (150 nm spacing) x16 base dose (200 nm spacing) x24 base

In this vein, new samples of thick Ag films deposited onto SiO2 were prepared with a remarkable change in the system recipe where the sputtering power was increased to 120W. One sample was selected to be loaded into E-Line system. The resulted

patterns shown in (Figure 10) refer to the four standard patterns that assumed in this research for each sample of interested where features in A, B, C & D were exposed to 1, 2, 3 & 4 dose factors, respectively. It is apparently that exposure dose of factor 2 & 3 gave the best and more optimising features as compared with other two patterns. For deeper details, (Figure 11) demonstrates the nanoscale morphology for the dots obtained from different separation distances and doses exposure. This part of the experiment clearly shows the polycrystalline structure for the thick Ag film with grains of various size distributions. This crystalline surface helped to success the process of imprinting uniform and consistent nanoscaled dots. Although some dots are missing as shown in (Figure 11A), it is still interesting results because these dots could be missed according to variation of the beam current value during the imprinting process. It also can be noticed notably that increasing the exposure dose for two patterns of same separation led to decrease the imprinting precisely and controllability of EBL within such conditions. Accordingly, optimum results can be accomplished from patterns of 100, 150, 200 nm spacing with exposure of 9, 16, 24 times base dose, respectively, where the base dose was 5μC/cm^2 in this experiment.

The obtained results are in agreement with another study by (Dutheil, Thomann, Lecas, Brault & Vayer, 2015) who illustrates that depositing Ag films of thickness above 16nm motivated 3D island formation with visible large grains of various shapes and sizes. There is a linear increase in grains size with increasing the film thickness (Kapaklis, Poulopoulos, Karoutsos, Manouras & Politis, 2006). The reason for this phenomenon as evidenced by Jing et al. is relating to the fact that 3D islands are arranged into several fragments closed together and separated by visible boundaries which gave the scanned surface a polycrystalline profile (Jing et al., 2009). It also reported that the first deposited layer seems to be unstable when the other layers start growing, which could be linked to fact of leaving some Ag atoms from the initial layer to next layers to form random grains shapes and sizes and, consequently, the polycrystalline appearance (Glueckstein, Evans & Nogami, 1996). From this part of the study, the influence of the surface morphology by the film thickness and the sputtering power was emphasised.

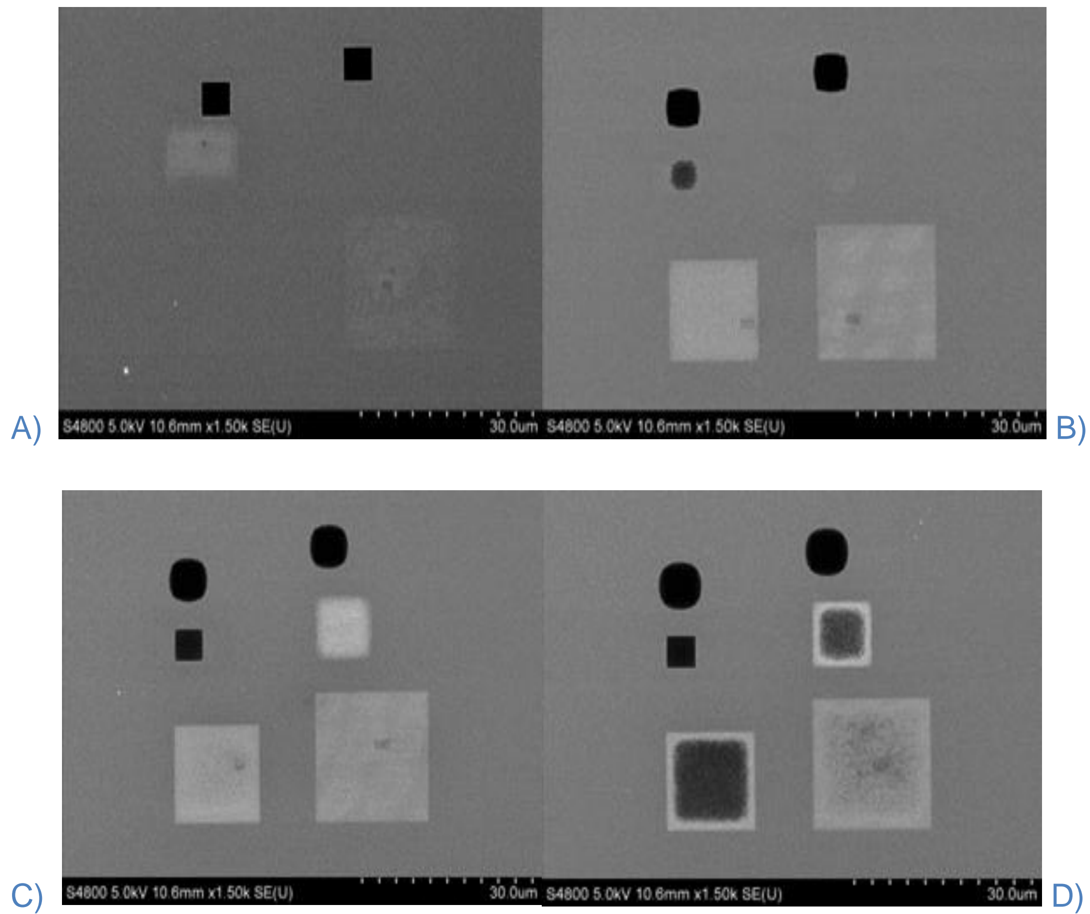

Figure 9 SEM scan shows the patterns on 20nm AG thin film deposited onto SiO2 with various dose exposures. A) Factor 1. B) Factor 2. C) Factor 3. D) Factor 4.

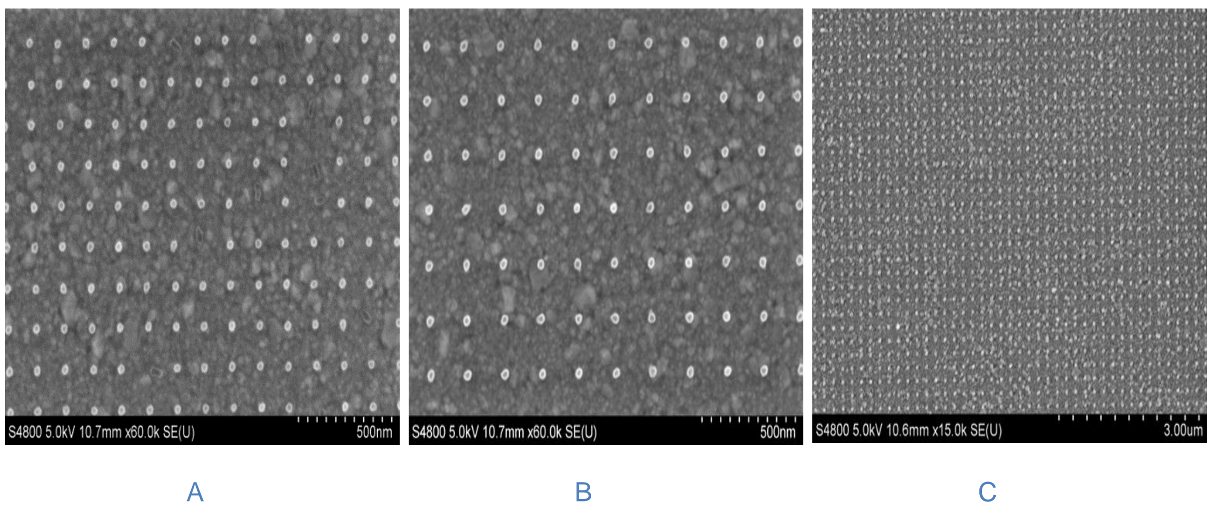

Figure 10 SEM scan explains for: A) 150nm spacing of 16 times base dose exposure. B) 200nm spacing of 24 times base dose. C) 200nm spacing of 36 times base dose.

A wet etch process was carried out to create a sample of silver nanodots supported onto SiO2 substrate. As mentioned before an acidic aqueous was prepared by mixing three strong acids with water. The etch rate was fast and uncontrolled because the first concentrated solution was very active and incompatible with the size of samples used. The second diluted solution was initially under control and presented good rate of etch when it was fresh. However, when it left a while until preparing another sample, the rate of etching became very slow, not uniform and could observe the etched silver clearly around the sample edges but not in the centre of the sample. This could be related to aging of the etchants since they underwent a strong interaction according to their activity. The wet etching process of silver has been explained by other researchers as the hydrophilicity nature of Ag thin films leads to peel off the interface surface due to loss the adhesion ability between Ag and the support sample (Ceyssens & Puers, 2009). Therefore, wet etch in case of silver requires many attempts with different etchant solutions relying on others experiences to achieve successful and controllable etch results.

To continue the investigation in terms of creating silver nanodots for catalytic reactions, a lift off process was conducted. Although a good morphology of 20nm silver film thickness was attained, a challenge of getting stable nanodots still remains. To tackle this problem, two lift off attempts were tried, as mentioned before. In the first run of this experiment, a thick C4%PMMA resist was deposited onto the patterned sample by spin coating. As shown in (Figure 6), a wide range of visible wavelengths can be observed that refer to various spreading thicknesses along the sample which affect the light interference reflected from different layers. The major appearance of the features obtained after depositing Ag metal and lifting off the resist were meaningless for whole doses used (Figure 12). These images also indicate that massive quantities of PMMA residuals were not lifted off which caused unclear features with peeling off the silver thin film elsewhere from the exposed surfaces.

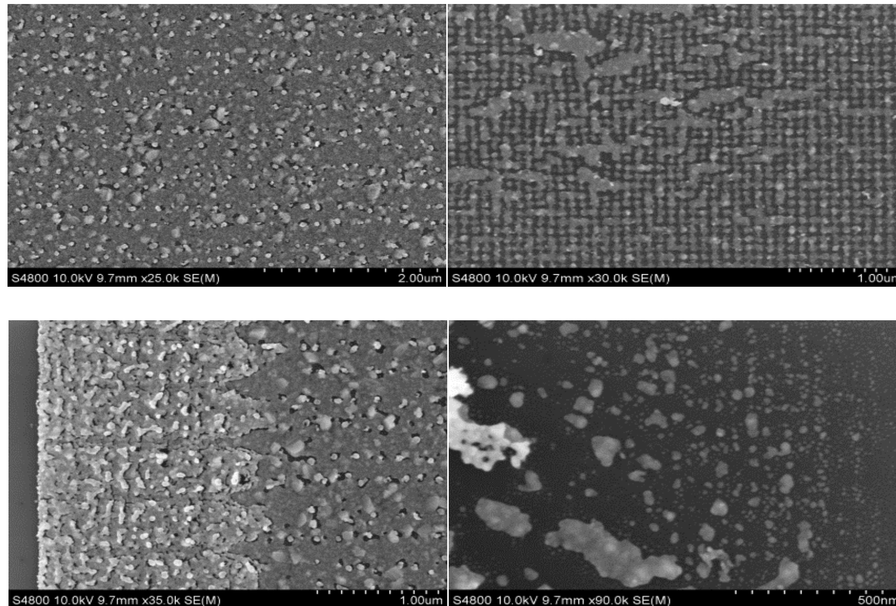

Figure 11 shows sample surface, PMMA residuals and irregular Ag patterns by employing lift off method with C4%PMMA

In the second round of lift off experiment, the resist was diluted to become C1%PMMA with less thickness than before. The performance of the new resist gave substantially important results. As illustrated in the previous section, the patterns were arranged into two rows of 20 arrays each. The first nine features in the top row were completely disappeared. These features were exposed to 1 to 9 dose factor of the base value which was 0.0001pC, while the patterns of factor 10 to 20 were obvious. Accordingly, no SEM images were presented for these patterns from the top array because the same dose factors can be found in the bottom array features. Figure 13 shows the uniformity and regularity of nanodots arrangement for a broad range of dose exposure factors. The main dose value of this row was 0.0001pC also, and the first pattern was exposed to double of this value where the second dose factor supplied to the next feature was fourfold i.e. 0.0004pC and so on. The first four patterns were entirely missing, but the fifth one of dose factor 10 was clearly seen which had the same dose value with the tenth pattern of the top array (Figure 13A&B). These images describe two dots arrays with different separation distances of (50 and 100) nm of total exposure dose of 0.001pC. The resulted dots were extremely encouraging even though some missing dots within the both patterns which could be related to little fluctuation in the value of the beam current during the imprinting period, or because the dose amount is very low with respect to PMMA thickness which expected to be not adequately uniform along the sample.

Meanwhile, size distribution of the obtained dots was between about (6-9) nm which is the smallest size could gain from the liftoff method with this particular spacing. From another study, the size of Ag metal dots that obtained by lift off on Si wafer was restricted to about 10nm with the possibility of adjusting the nanoparticles spacing from 200 to 10µm, typically (Henry, 2014). Moreover, quite best results can be found in (Figure 13C, D, E and F) where increasing the exposure dose led to increase the uniformity and clarity of nanoparticles. The feature of smallest spacing (50nm) seems to be affected by the proximity effect which significantly appears with high doses and small separation distances between nanoparticles. However, increasing the spacing with keeping the exposure constant generally resulted in perfect and regular distributed dots. An important indication can be noticed when the separation distance broadened; the size distribution of particles was markedly decreased, which also can be detected by the high magnification power used with enlarging the spacing. Another key point importantly mentioned here that there is a linear relation between particles size and exposure doses, where the distribution size of the nanodots in (Figure 13C) was tripled to about (17-26) nm with doubling the dose factor as compared with (Figure 13A). Extra exposure doses continued giving appropriate results, except the pattern of 50nm spacing with dose factor of 40 due to the proximity effect. (Figure 13G & H)

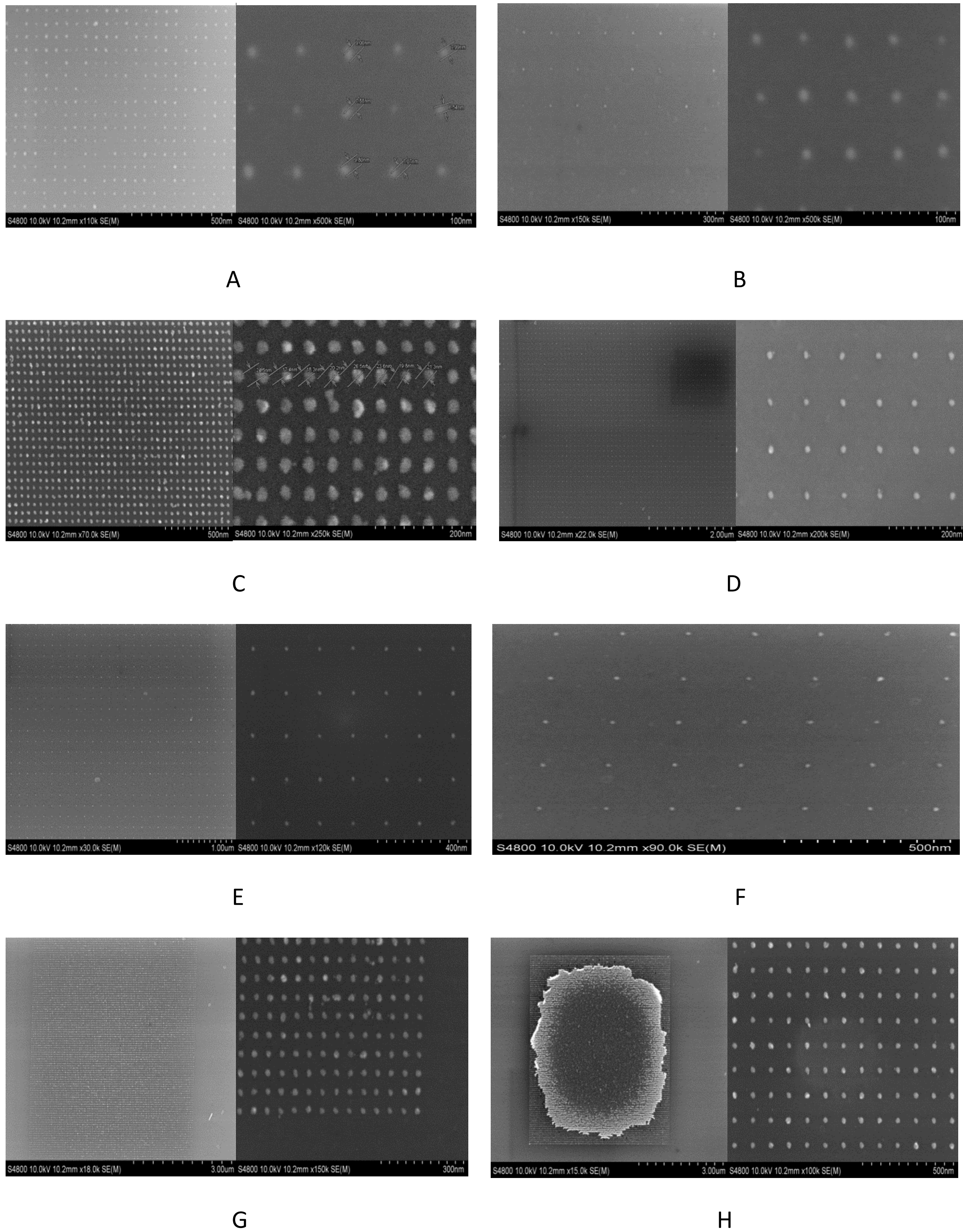

Figure 18

Figure 12 presents SEM scans for nanostructures after lift-off C1%PMMA photoresist: A) 50nm spacing of 10 dose factor. B) 100nm spacing of 10 dose factor. C) 50nm spacing of 20 dose factor. D) 100nm spacing of 20 dose factor. E) 150nm spacing of 20 dose factor. F) 200nm spacing of 20 dose factor. G) 50nm spacing of 22 dose factor. H) 50 & 100 nm spacing of 40 dose factor.

Surface analyses were conducted by X-ray photoelectron spectroscopy XPS model (AXIS SUPRA KRATOS ANALYTICAL). The sample of interested was loaded along night time to pump down the interior pressure of the system. Figure 14 shows a diagram of the XPS spectrum, which displays peaks of silver metal into different electronic states, contaminants that could be indicated to resist residuals or dirt from tools used during the fabrication steps, and also peaks of silicon and oxygen into various densities of states. These analyses were done before cleaning the sample. Therefore, it can easily explain the presence of carbon atoms in the spectrum due to PMMA organic resist that used as a sacrificial layer for lithographic patterns. A very low amount of fluorine peak can be observed as well, this could be attributed to a little amount of impurities remain in beakers or other tools used in lift off procedure. Major emission peaks were from oxygen molecules from different energy levels. This phenomenon is simply specified the oxygen bonds with silicon and silver atoms to generate metal oxides. Basically, the metal dots produced by lift-off approach are not really pure and a serious demand for cleaning surfaces is essential. Cleaning is commonly run by applying the samples to the oxygen plasma system followed by a high temperature annealing either under ultra-high vacuum chamber UHV or with the presence of oxygen, however, treating silver via this way can significantly affect the shape of the metal particles (Henry, 2014).

Although the impurities were not of extremely high quantities, cleaning was implemented. The aim of cleaning process was to remove carbon residual which was comparatively much less than silver metal amount (Figure 14). Again, the purpose of this study, as mentioned earlier, is to fabricate silver nanostructures to be exploited in diverse catalytic applications. Thus, the cleaning is necessary before been used as catalysts (Henry, 2014). Because of the limited time allocated to finish the research, a one type of cleaning treatment was followed, in which the previously tested sample was loaded into O2 plasma chamber. The benefit of this process is to generate mono or dioxide carbon gases which evaporate from the surface to leave the sample completely pure, but with a serious issue of creating silver oxide compounds. To tackle this problem, a dry etching process or hydrofluoric acid HF can be applied utilised after plasma cleaning. Unfortunately, the obtained results were unexpected because of the partial peeling of AgNPs from the surface. This could be improved by annealing at high temperature (Henry, 2014) or increase the

adhesion ability for Ag to SiO2 substrate by depositing an interfacial thin layer of chromium or platinum (Xu, Tang, Shao & Fan, 2005).

3.4. Conclusion

To conclude, many attempts were tried to get the best film morphology of Ag metal by altering either the conditions of the physical vapour deposition system PVD or the concentration of the photoresist used in lift-off method. Wet etching and lift-off methods were used to fabricate silver nanoparticles AgNPs which imprinted with using Electron Beam Lithography EBL technique. Two Ag thin film thicknesses about 10nm and 20nm were deposited by PVD, specifically; DC magnetron sputtering mechanism. The wet etched samples were given non-uniform etching rate and then, unclear features with dissolving a quantity of Ag metal into the etchant mixture. A comparable approach has been achieved from 20nm film thickness, roughly, with a good distribution of uniform nanodots array by adopting C1%PMMA resist for the lift-off process, which presented the smallest nanoscale dots less than 10nm, yet.

.

Figure 13 displays XPS spectrum for surface compositions after lift-off process

Chapter 4

Manufacturing of nanostructured Features by SCIL technique

4.1. Introduction

Substrate conformal imprint lithography (SCIL) is a novel technique for full template scale nanoimprint lithography to transfer nanostructures from a PDMS stamp into AMONIL which is a resist of low viscous organic/inorganic composite substance [2]. A curing process is needed to promote the patterns formation. The curing process either conducts by Sol-Gel diffusion through PDMS or by UV-enhanced treatment UV-SCIL. The curing times for the both approaches are limited to be (3-15) min. A wide range of applications are well controlled by these methods, but a key limitation is evidenced regarding their partial inorganic nature which restricted their efficacy with other processes (Schmitt et al., 2012). Some competing solutions to improve UV-SCIL performance were investigated. A study has introduced an alternative material to be suited for various industrial applications with curing time of 17min. The innovated UV-curing materials are purely organic which and showed a significant increase in the process throughput. To ensure a stamp maintenance, high imprints number and high stamp quality, the interaction rate between the PDMS material and the UV-curing resist should be kept low as much as possible to avoid features deformations (Fader et al., 2012)

The present study aims to go through the sequential steps of the SCIL technique as a preliminary work for future projects in field of configuration nano scale structures. Thus, this chapter will focus on some challenges that could limit the accuracy and imprinting efficiency. This chapter could appear unrelated to the main purpose of this project, but in fact, there was an intention to create arrays of nanodots on a large wafer to be used in preparing microchips for the best results gathered from experiment 1. Unfortunately, lack of time was the only drawback to invest in this opportunity. For research purpose, this technique was implemented to imprint silicon nanowires instead of Ag due to availability of SNWs mask, and it is easier to use silicon substrate alone without any deposited metals to save time.

4.2. Materials and methods

(1) Master wafer preparation:

A 4” Si wafer was cleaned manually with acetone and API solvents and dried with nitrogen to be ready for coating process. A thin layer of AZ6612 photoresist was deposited on Si substrate by the spin coating system (WS-650MZ-8NPP/A1/AR1) under operating conditions of: (3000rpm) the rotation velocity and acceleration of 1000rpm/s for 45s. Then, a metal plate was heated till 100˚C to bake the sample for the 90s. The coated wafer was exposed to UV-light after locating a transparent mask of nanowires features between the sample and the UV source (SUSS MicroTec MA8) which also called mask aligner system. The exposed dose was 250mJ/cm2 for 10s. Next, the patterned template was developed by the AZ MIF726 developer to remove the exposed resist. The developing process was carried out by immersing the sample into the developer for (30-60)s followed by rinsing with DI water and then blown dry with nitrogen. The final sample was dried etched by (SPTS ICP) Inductively Coupled Plasma Etch system. The etchant gas used was sulphur hexafluoride SF6. Thus, the sample was loaded off and intensively washed with acetone in an ultrasonic bath (Fisher brand FB15063) to remove the remained resist. Figure 15 shows the master wafer after cleaning with a clear appearance for the patterns. It is obvious that the resist not completely removed and still some residuals which seem as dark areas on Si wafer.

Figure 14 shows a photographic image for the master wafer after cleaning with visible patterns

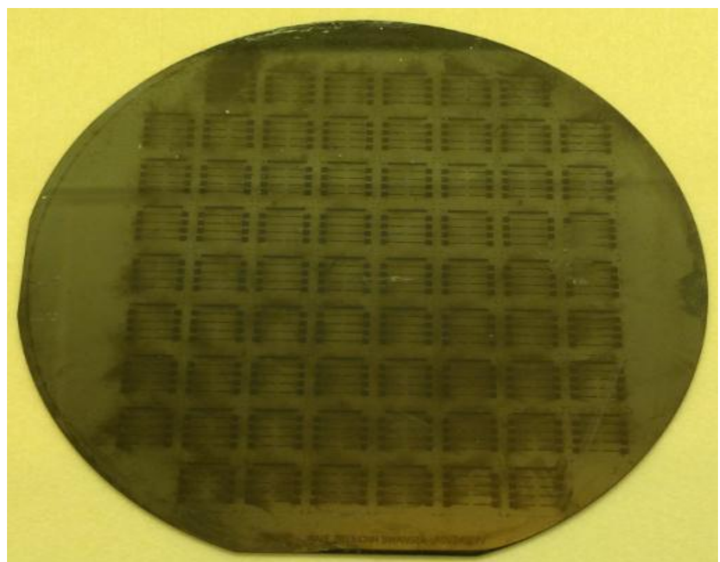

(2) Evaporation of FDTS thin layer:

A monolayer of Perfluorodecyltrichlorosilane (FDTS) was deposited by vapour phase deposition onto the prepared master, which acts as anti-sticking layer to prevent adhesion of the stamp material PDMS to the sample surface after replication stage. A few drops of FDTS solution were poured into small beaker and immediately put in a desiccator bottom due to its high volatility. Finally, fixing the sample (face- down) by a holder of three arms hanging to the desiccator lid from inside was carefully done. Lastly, loading the whole system under vacuum of about 10-2mBar into a hot oven (Genlab INCUBATOR) of 50˚C for over than 12h.As shown in Figure 16, the coated wafer with the anti-sticking layer led to generate a hydrophobic molecule which obviously affected the interaction of DI water drops with the top layer.

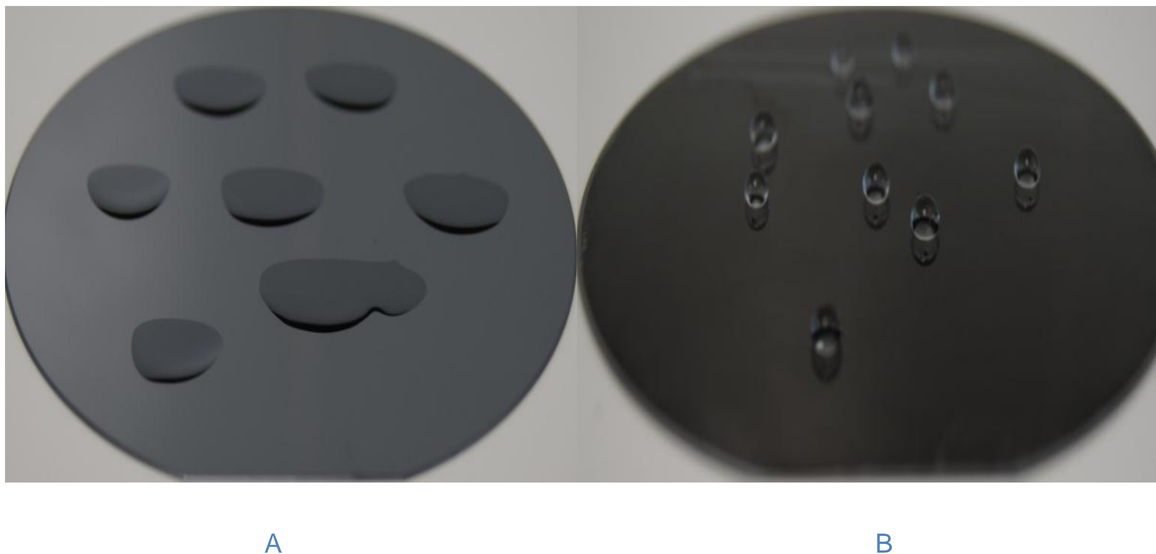

A B

Figure 15 photographic images show the effect of the anti-sticking layer FDTS on DI water droplets.

(3) Replication of PDMS mask rubber:

A soft PDMS 184 rubber was prepared by mixing (10:1) g of silicone elastomer with curing agent which shaken thoroughly for 2min. Degasing the product within the desiccator into the oven at 50˚C for about 15min to ensure the removal of all bubbles trapped between the solution molecules. Only 5.2g was needed to mold the required PDMS mask onto the master.

A thin glass sheet of suitable size to the 4” wafer was etched by 1%HF for 60s for each edge. Then, preparing the master replication tool MRT was carried out by cleaning the glass carrier (AF45 Schott AG) with acetone and IPA and rinsed with DI water. The glass carrier surface was wiped with a pre-adhesion layer of PDMS-Primer Dow Corning 92-032 and wormed up to 50˚C to prevent sticking of the stamp with its holder at the end of the replication process. SCIL technique requires a fully cleanliness to inhibit defect generation which causes features failure. The master carrier was also cleaned with IPA before loading the wafer. The MRT heater was turned on up to 50˚C after refilling the chillier with water required to be circulated through microchannels to spread heat along replication period. The master wafer was aligned to the MRT metal template with attempts to keep it completely flat, and this step followed by dispersing 5.2g of PDMS, which previously prepared, onto the centre of the master, carefully. Finally, a vacuum was applied to the system to keep the glass sheet and the master stable during the molding process, and then the glass carrier was closed manually with keeping an initial gap between the carrier and the PDMS layer to be adjusted carefully by three micro screws on the top of the lid. To ensure acquiring on a solid rubber material, the system was left for more than five days with daily observation and checking for the MRT circumstances such as its water amount, temperature and pressure.

After the fifth day, the rubber mask became solid enough to be used for the consequent UV-SCIL steps. To ease the separation process, the rubber edges were carefully undercut for about 1mm along the sides with keeping the cutter away from the glass material. Releasing the stamp from the wafer was controlled carefully by using a mechanical separator to avoid damaging the glass sheet or the features themselves.

Figure 16 displays the rubber stamp on a glass sheet with a black rubber ring

Features on the stamp were inversely replicated with respect to the master used. To finalize this step, a flat rubber ring was cleaned and stuck to the glass sheet by using good quality glue to ensure good adhesion results (Figure 17). Finally, table 9 summarises the replication steps of the PDMS mask material with some hints.

(4) Preparation for UV-SCIL exposure:

Two 6” Si wafers were cleaned and coated with two resist layers. The first layer called Amoprime, which acts as a good adhesion layer between the Si and the next layer, with a thickness of ~10nm. The spin coating regulator was set into following conditions for the both layers: rotation velocity of 3000rpm with acceleration of 1000rpm/s for 20s, and then warmed up to 80˚C for 60s. The template was left to cool down before depositing a thick layer of the second resist which is named AMONIL MSS1. A SUSS MicroTec SCIL system was employed for the UV exposure and imprinting the nanowires chips.

The principle mechanism of imprinting PDMS rubber into sol-gel resist is schematically illustrated in Figure 18. To confine the gap and keep the stamp close to the substrate, the grooves existed within the stamp holder are typically pressurized with (15-30) mBar. An overpressure starting initially from one side is loaded to the first groove. This pressure causes swelling the stamp underneath the pumped groove, and consequently, forming elevated lines parallel to the grooves. Continuously, the neighbouring grooves are sequentially pressurized and the stamp will gradually attach the substrate by bridging the gap. The exposure time permits the stamp to be in contact with the wafer until hardening the resist layer. Afterward, the stamp is liberated from the created features by gradual vacuum evacuation from the grooves from the same side which attached first (Vershuuren & van Sprang, 2012).

The instrument was very well guided by following the hints that appear on its digital screen after each step. There are two modes to operate the system: single SCIL and multiple SCIL. The first mode was used in this experiment because the second mode suited for complex fabrication features with multi-directions imprint. A blank substrate without coating resist was loaded into the wafer holder, and the prepared mold was fixed into the mask holder of this system. Firstly, the gap distance between them was

aligned to 100µm to determine the zero position. The operation recipes were 850W for UV power, 3KP for the system pressure and the exposure time was 540s.

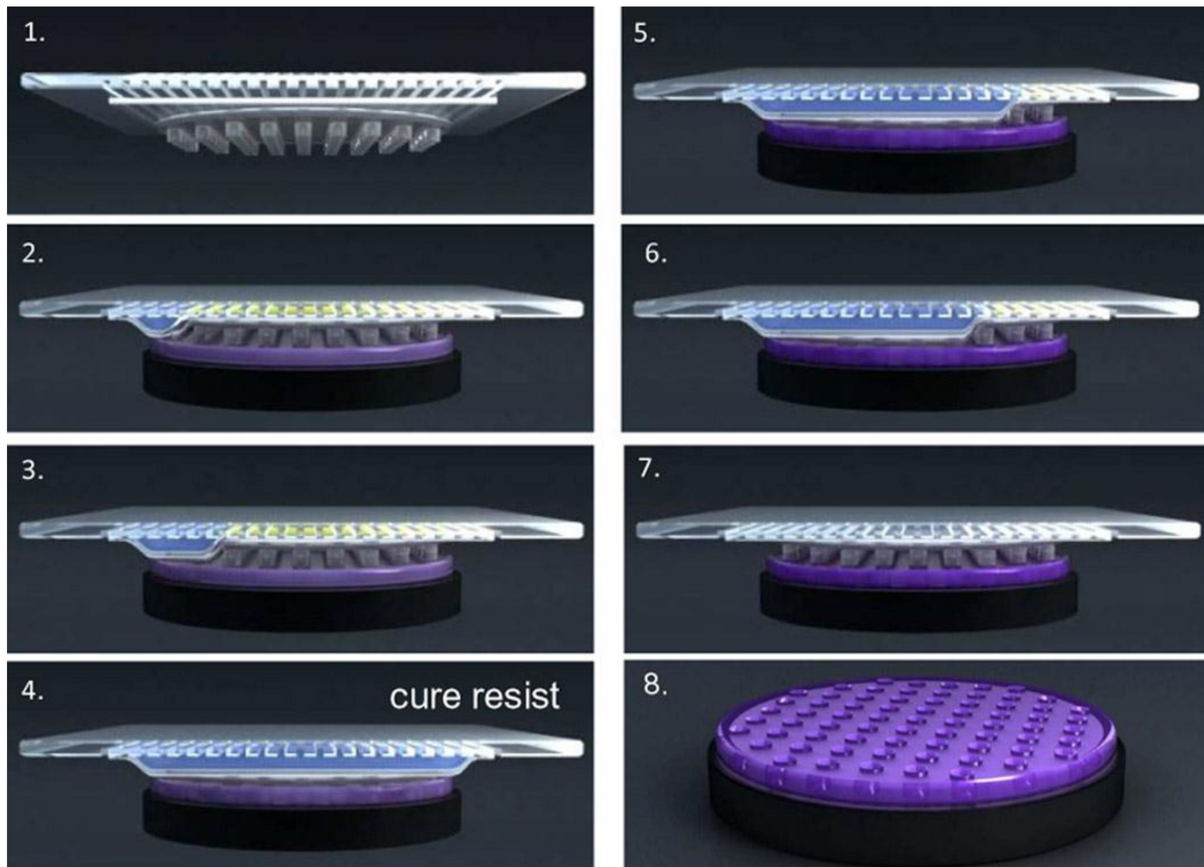

Figure 17 illustrates schematically the basic steps for the substrate conformal imprint lithography technique (Vershuuren & van Sprang, 2012)

Accordingly, And after setting the recipes, the coated wafer with AMONIL resist was loaded instead of the blank sample and aligned to the zero position. The following step after the alignment was imprinted the stamp into the thick resist layer and then curing the resist under UV light with over exposure dose. The obtained patterns were adequately good as compared with EBL technique in terms of features number and the large imprinted area. Figure 19 demonstrates the major surface features of the wafer after the UV-SCIL process and the patterns are concentrated on one side only.

Consequently, another endeavour was tested to promote the results. The separation gap distance was decreased to 90µm as a way to increase the patterns penetration into the sample. The second wafer was loaded with similar recipes except the zero position. However, the results were not better than before. Figure 20 shows the

sample sample appearance after decreasing the gap distance which introduced a few central patterns with an obvious boundary from the stamp edges.

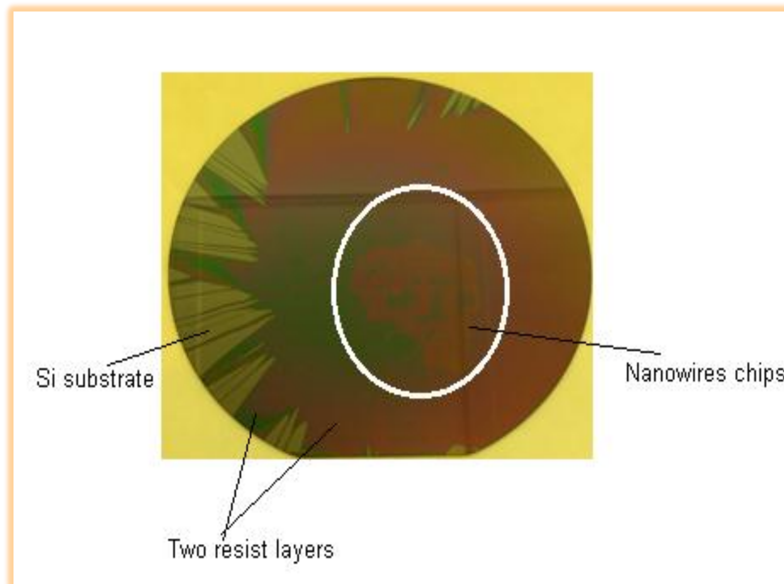

Figure 18 presents the final appearance of the imprinted wafer at 100µm gap

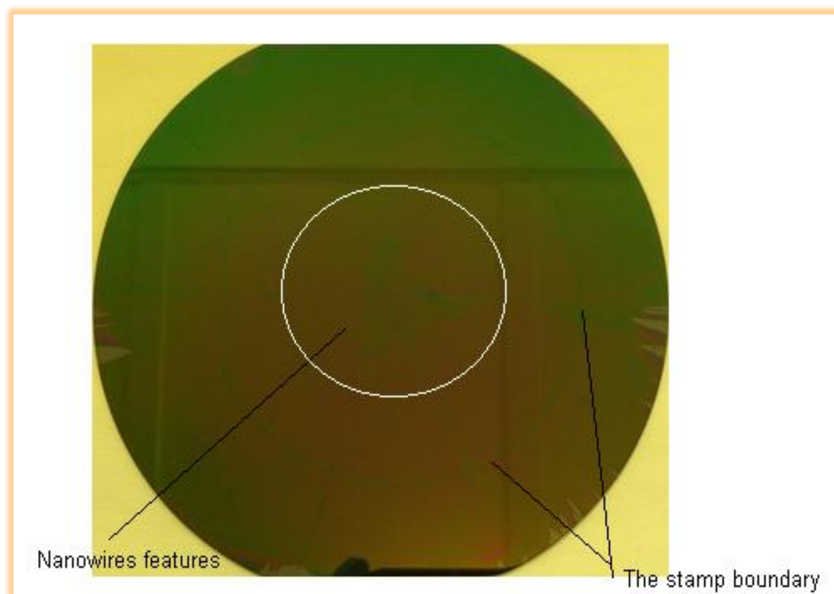

Figure 19 shows the final appearance of the imprinted wafer at 90µm gap

Table 9 summarises the replication steps of SCIL 4”- Stamp

Action	Parameter	Hint
Mix Soft-PDMS parts PDMS184 : Curing Agent (2 pipettes)	10.0 : 1.0 (g) needed: 5.2g	mix solution thoroughly for 2 minutes
Degas Soft-PDMS in a desiccator	Takes about 15min	Caution: Overflowing at the beginning possible. Shaking helps!
Etch edges of glass with 1%-HF	60s each side	Use HF-Pool
Clean glass carrier (AF45 Schott AG)		Rinse Acetone, Isopropanol, Di-H2O
Apply PDMS-Primer Dow Corning 92-032		Wipe from centre to outside
Put glass carrier in Oven	50°C	
Clean MRT thoroughly		Use Isopropanol
Turn on the Heater/Chiller of MRT	50°C	Refill Chiller with Di-H2O if necessary
Place glass carrier on Replicator; Turn on the vacuum		Check the vacuum again. Blow the surface of glass carrier.
Place master on the MRT		Use metal template to align
Disperse Soft-PDMS onto the h-PDMS	5.2 [g]	Central and very close to the surface.
Adjust the three microscrews	-3.2 mm	Avoid contact while closing the lid manually. First contact probably at -2.0 mm
Press the glass carrier very slowly on the PDMS by using the microscrews		Slowly and even to prevent surface from air bubbles
Cure the template in the replicator for 5 days	50°C	
Refill heater with Di-H2O every 2 days		
Release vacuum and carefully remove template from replicator		N2-pistol and Cleanroom-Cloth can be very helpful
Remove master with separator tool		Use additionally scalpel and Ethanol
Trim the edges	1-2 mm	
Clean black rubber flap ring (FKM75 Eriks Bayern GmbH)	240x240 mm	Di-H2O only.
Glue the rubber flap ring on the glass carrier		Use e.g. UHU Plus. Glue 5 mm of the edge of the carrier glass
Wait for glue drying	~6 hours	Make sure bottom of stamp is not sticked to cloth or table beneath

4.3. Results and Discussion

The first wafer of 100μm gap distance with the stamp was only chosen to be analysed by SEM. Firstly, cutting the wafer into several small samples of clear and best imprinted features was done before loading them into SEM for top-down and cross section imaging.

For the first investigation, SEM analyses were collected to identify some of the potential reasons that gave non valuable results. Figure 21A presents top-down views of one of the clearest and most perfect features created in this experiment.

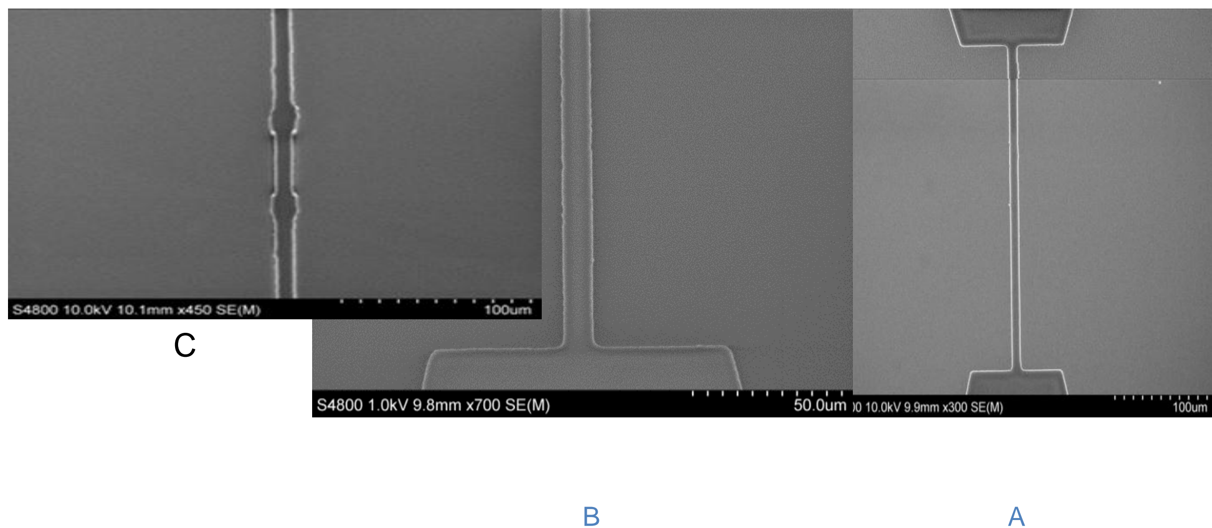

B A

Figure 20 SEM images for: A) perfect SiNW, (B&C) a microchannel with defects

Arrays of silicon nanowires were somewhat observed with high quality and uniformity while other patterns were evidenced with defects (Figure 21B and C). Although the features produced showed insufficient imprint quantity and quality, the evaluated measurements for the obtained pads and their channels for most SiNW structures were appropriate and consistent. Figure 22 demonstrates some optimum dimensions for SiNW parts. The size of the wider parts (pads) was around 200μm and the width of measured microchannels was between (9-10) μm.

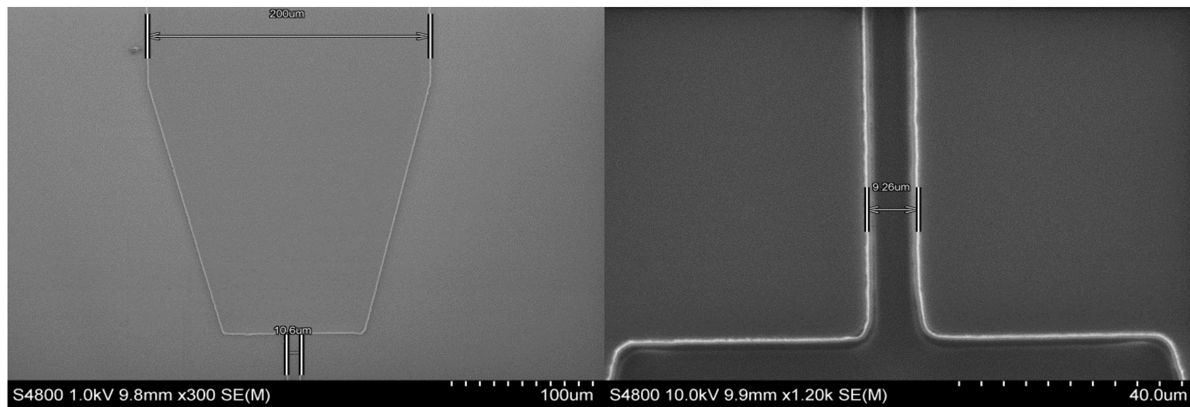

Figure 21 evaluates the dimension measurements for most SiNWs measured by the aid of SEM skills

For the second investigation, cross section scans for the prepared samples were studied. Figure 23 indicates the accuracy and clarity of features formed by SCIL technique. The micrographic images A&B in (Figure 23) show an obvious microchannel linked to the wide component of a SiNW pattern and its depth through the organic-inorganic resist on the Si substrate, respectively. The resist residual thickness and the total deposited thickness of Amoprime + AMONIL layers were calculated. As noticeably shown in (Figure 23C&D) that the thickness of the non - removal layer is several nanometres ~231nm while the total layer thickness is nearly (750-850) nm. Thus the massive difference between the two thicknesses triggered the formation of sharp edges which refers to the sol-gel material compressed during the patterning process by the UV exposure. The top black surface is an evidence of influencing the resist polymeric materials by the negative charges from the electron beam current and then creates a charged layer which gives imprecise thickness value. However, the resist layer remained on the imprinted features is optimising and could be removed easily by a suitable etching process, not within the scope of this study.

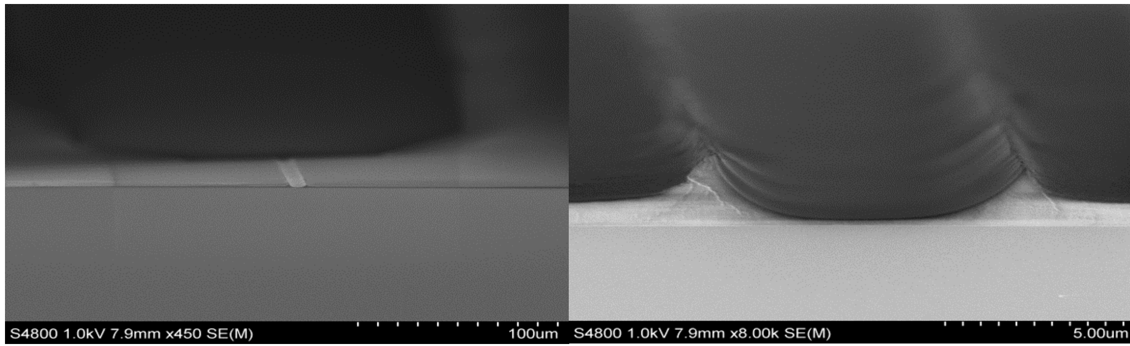

A B

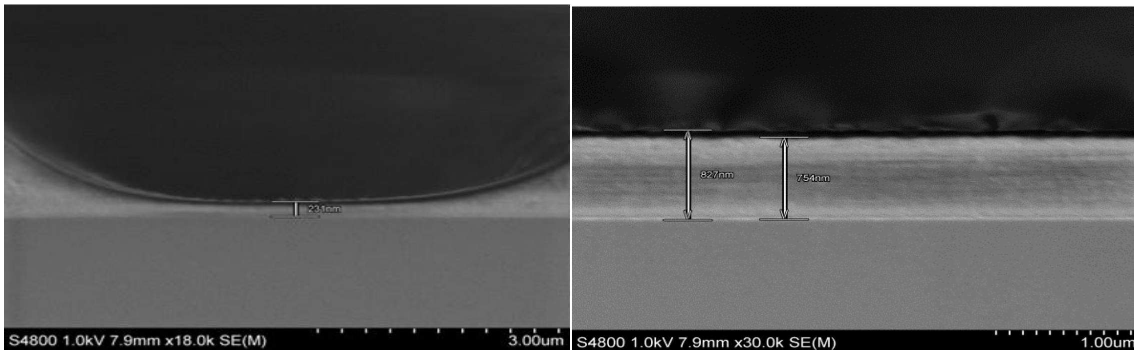

C D

Figure 22 displays the cross section analyses by SEM: A) one end of a microchannel with its pad B) zoom in the channel cross section C) the resist thickness remained on features D) the total thickness of the deposited resist

To assess and specify the reasons of formation undesirable results, it is essential to identify the defect and at which step it could be happening. Accordingly, it has been reported in the literature two sorts of deformations: incomplete feature replication and particle related defects which are both mainly presented with a hard stamp rubber (Verschuuren, 2010). However, and as evidenced from this experiment, the formation of bubbles in different sizes randomly on the stamp was a probable cause for giving incomplete imprinting on the wafer. In addition, the undercut sides of the stamp need to be controlled mechanically not manually to ensure the symmetrical edges for the entire mold. Figure 24 clearly shows how the asymmetrical stamp edges prevent a complete attach between the stamp and the substrate which led to produce central features only. Whereas, the reasons which related to particle defects could be illustrated according to Figure 15 as it remarkably displays the Si master wafer with totally defective surface regarding to the resist particles remained after

etching. These residuals were possibly resulted in incomplete, weak and unreliable features on the rubber which, consequently produce undesirable SiNW designs. As mentioned before, the process that adopted in this investigation was soft lithography technique in which the stamp removal is simply to be achieved, but with a drawback of stamp deformations like pairing/ sagging which restrict the resolution value and placement precision (van Delft, van de Laar, Verschuuren, Platzgummer & Loeschner, 2010)

Furthermore, some operating recipes could have a direct influence on patterns imprinted by SCIL technique such as the gap or zero alignment distance, the applied force on the mask, groove pressure and substrate temperature. As proved earlier that decreasing the gap distance gave less features number with an obvious stamp edge, or in other words, increasing the imprinting force regarding this shrinkage under the same operating conditions with the large gap experiment. This relation could be explained due to low Young's modulus of PDMS rubber which enables an ideal contact between stamps and substrates (Verschuuren, 2010), as a result, the stamp bending at the end of the 90µm gap examination was clearer and larger than that at 100µm test. Additionally, increasing the substrate temperature to some extent over room temperature by heating up the wafer holder during the curing process decreases the exposure time, and also elevating the stamp depositing speed can accelerate features filling process because the viscosity of the resist materials decreases at high temperatures (Fader et al., 2012). This innovative work would promote the SCIL technique and then advance chips integration industries by its feasibility to produce enormous tiny patterns onto large area in a short time.

Moreover, other researchers have explored that the interaction between components of the UV- curing materials with PDMS influences by the diffusion permeability of the stamp surfaces. This interaction can be classified into three scenarios: no interaction occurs during the exposure time, swelling the PDMS surface which could lead to markedly change in patterns shape, or degrades the stamp surface which would increase the separation forces and then cause patterns damaging. Any of those theories has a concern about the accuracy of transferring patterns, as well as, the total lifetime of the PDMS rubber materials (Schmitt et al., 2012). Fader and his colleagues reported in 2012 that not all the investigated materials are chemically

compatible with PDMS mask for soft imprint lithography technique. Some of them are strongly adhered to the mask material after the curing process, while others are ultimately not cured during the exposure to the UV source which could be attributed to formation an inhibition layer of oxygen absorbed by the PDMS surface from the atmosphere (Fader et al., 2012). Therefore, the chemical harmony between the mask material and the imprint resist should be taken into consideration.

4.4. Conclusion

Generally, the results obtained from SCIL technology were slightly undesirable. Although the larger quantity of features exposed on wider wafer than that yields from EBL, the nanostructures morphology was irregular with numerous defects has been detected by SEM images. Two gap separation distances between the wafer and the stamp were examined which introduced the same quality of feature yield. The main key point for successful and efficient SCIL results is contaminations and stamp deformations which should be taken into consideration for each step of preparing a master to molding a stamp to SCIL system recipes.

Chapter 5

Conclusion and Recommendations

5.1. The Conclusion

Nanotechnology has a significant impact on developing the most recent applications such as electronics, photonics, environment, medicine and also catalysis reactions. Enormous advances in catalysts synthesis domain a great interest in many scientific research and publications. Ag metal has attracted a major attention regarding to its significant characteristics of extremely high thermal and electrical conductivity in addition to high reflectivity properties. The present study elucidated the catalytic properties of various metal-based catalysts and some factors that influenced their selectivity and activity. Catalysis reactions are substantially influenced by the size, shape, structure, material of the catalyst particles. Innovative methods for nanocatalysts synthesis have evidenced a significant key role in promoting their catalytic performance. Some common fabrication techniques have been highlighted in this study, such as electron beam lithography and substrate conformal imprint lithography.

This research has dealt with two major techniques as a preliminary stage to fabricate a catalyst of nanodots arrays in the future. The larger part of the current thesis is fabricating uniform and consistent nanoparticles rather than randomly distributed on a substrate. Silver nanodots were created by depositing different thicknesses of silver thin films onto SiO_2 by using the PVD technique. Various attempts were tried on the silver and SiO_2 surfaces to achieve the optimal thickness. Exclusively, the smallest dot size has been observed in this research about (6-9) nm with desirable uniformity and distribution. This result can be obtained from Ag film of thickness about 20nm, C1%PMMA positive resist used in lift-off method, and imprinting the features by E-Line lithography with exposure charge about (0.002-0.008) pC. The main reason of the lift-off preference is the weak yield that obtained from the wet etching for silver film and contributing a non-uniform etching rate with vanishing the patterns.

The second aim of this research is adopting a slightly complex technique rather than EBL to create silicon nanowires as an initial approach to fabricate silver nanoparticles. The gathered results were, to some extent, acceptable. However, it is comparable and compete EBL in terms of providing high pattern throughput for large area within a short time. Importantly, this technique requires much more control and

careful attention than other replicating techniques. The key point is keeping the mask, wafer and master substances completely free of contaminants and from the formation of mask deformations and defects. It is worth explaining that the thick resist layer of AMONIL led to inadequate purity for the features created because of the resist amount that left behind after imprinting. An optimising approach can be achieved by controlling the resist thickness.

5.2. Future Research

The major limitation that faced the progress of this research was the time factor. Interestingly, it was expected to adopt a research in CNH of a hybrid strategy combines between the optimisation achievements obtained from the both technique EBL and SCIL. The basic objective is to synthesise a nanocatalyst of silver nanodots arrays deposited onto different substrates which are created by EBL with particle size and spacing of 25nm. The benefits of utilising SCIL is to produce a model stamp for these nanodots to be replicated into multiple wafers to save time with less cost and high throughput. This promising research could be a breakthrough in the field of nanocatalysis reactions with a potential advancement in the domain of nanoimprint lithography. It is a precious opportunity deserves to be investigated.

5.3. Future Work

Based on the difficulties that confronted the progress of this work, some suggestions and recommendations will be listed in this section.

- Because of the low affinity between the silver metal and oxygen, it could be better using an interfacial substance to enhance the chemical affinity of silver to SiO_2, supporting on other substrates, or annealing with adequate temperature.
- It could be helpful to deposit a thin silver film on SiO_2 by utilising RF magnetron sputtering or CVD, for comparison purposes.

- It is important to apply a sufficient sputtering pressure of argon used in the PVD chamber to deposit silver film equal to its optimising value of 2.5Pa (Dutheil, Thomann, Lecas, Brault & Vayer, 2015).
- It is essential to control the beam current for e-Line Raith system where the fluctuation in the current value affected the uniformity of particles distribution along the features with some missing patterns.
- In terms of wet etching, there was a big challenge of controlling the etching rate which significantly affected the patterns appearance. From the literature, either using dry etch in H_2 and CH_4 plasma (Choi & Hess, 2014), or using a wet etching approach by mixing 1:3 of HNO_3:H_2O which gives a remarkably low etching rate of 11nm/s (Lee, Bien, Badaruddin & Teh, 2012).
- As recommended by this research that employing the lift-off method gives an encouraging results, however, cleaning the sample after peeling the resist is a major issue. Organic contaminants with a massive oxygen quantity have been observed and cleaned by loading the sample in an oxygen plasma system, but this led to remove the silver patterns. To tackle this problem, annealing process at low temperature can follow plasma treatment, or cleaning the sample by using Dimethyl sulfoxide DMSO solvent at high temperature of 70°C. A gentle cleaning should be taken into account for both methods.
- To improve SCIL results, the main recommend is to keep all the set materials (the master, PDMS mask rubber and the wafer of interest) clean, prepared precisely by following the guide of SUSS system and check the Young's modulus for the PDMS, frequency, to detect any defect or deformation which has a significant impact on the imprinted structures.
- Thickness of the photoresist used in both techniques EBL and SCIL has a serious effect if it is thick enough to be remained after imprinting which totally leads to remove the features with lift-off or etching the resist, respectively. As a result, the thickness of the resist requires more attention to ensure good results.

References

A. Bhosale, M. and M. Bhanage, B. (2015). Silver Nanoparticles: Synthesis, Characterization and their Application as a Sustainable Catalyst for Organic Transformations. *Current Organic Chemistry*, 19(8), pp.708-727.

Ahmed, J., Sharma, S., Ramanujachary, K., Lofland, S., & Ganguli, A. (2009). Microemulsion-mediated synthesis of cobalt (pure fcc and hexagonal phases) and cobaltâ€"nickel alloy nanoparticles. *Journal Of Colloid And Interface Science*, *336*(2), 814-819. doi:10.1016/j.jcis.2009.04.062

Arve, K., Klingstedt, F., Eränen, K., Murzin, D. Y., Čapek, L., Děde˘ek, J., ... & Bovin, J. O. (2006). Analysis of the state and size of silver on alumina in effective removal of NOx from oxygen rich exhaust gas. *Journal of nanoscience and nanotechnology*, *6*(4), 1076-1083.

Arve, K., Svennerberg, K., Klingstedt, F., Eränen, K., Wallenberg, L., & Bovin, J. et al. (2006). Structureâˆ'Activity Relationship in HC-SCR of NO x by TEM, O 2 -Chemisorption, and EDXS Study of Ag/Al 2 O 3. *The Journal Of Physical Chemistry B*, *110*(1), 420-427. doi:10.1021/jp055147x

Baier, S., Rochet, A., Hofmann, G., Kraut, M., & Grunwaldt, J. (2015). Lithographically fabricated silicon microreactor for in situ characterization of heterogeneous catalystsâ€"Enabling correlative characterization techniques. *Rev. Sci. Instrum.*, *86*(6), 065101. doi:10.1063/1.4921775

Bhatt, P. A., Pratap, A., & Jha, P. K. (2015). Size and Shape Dependent Catalytic Activation Energy of Different Nano Structures.

Black, A., Paul, K., Aizenberg, J., & Whitesides, G. (1999). Patterning Disorder in Monolayer Resists for the Fabrication of Sub-100-nm Structures in Silver, Gold, Silicon, and Aluminum. *J. Am. Chem. Soc.*, *121*(36), 8356-8365. doi:10.1021/ja990858s

Brinker, C. J., & Scherer, G. W. (1990). Sol–Gel Science: The Physics and Chemistry of Sol–Gel Processing, Acad. *Press Inc., San Diego, USA*.

BRON, M., TESCHNER, D., KNOPGERICKE, A., STEINHAUER, B., SCHEYBAL, A., & HAVECKER, M. et al. (2005). Bridging the pressure and materials gap: in-depth characterisation and reaction studies of silver-catalysed acrolein hydrogenation. *Journal Of Catalysis*, *234*(1), 37-47. doi:10.1016/j.jcat.2005.05.018

Burch, R., Breen, J., Hill, C., Krutzsch, B., Konrad, B., & Jobson, E. et al. (2004). Exceptional Activity for NO x Reduction at Low Temperatures Using Combinations of Hydrogen and Higher Hydrocarbons on Ag/Al 2 O 3 Catalysts. *Topics In Catalysis*, *30/31*, 19-25. doi:10.1023/b:toca.0000029722.12588.1f

Ceyssens, F., & Puers, R. (2009). Deep etching of glass wafers using sputtered molybdenum masks. *J. Micromech. Microeng.*, *19*(6), 067001. http://dx.doi.org/10.1088/0960-1317/19/6/067001

Chang, J., Zhou, Q., & Zettl, A. (2014). Facile electron-beam lithography technique for irregular and fragile substrates. *Appl. Phys. Lett.*, *105*(17), 173109. doi:10.1063/1.4900505

Chaturvedi, S., Dave, P., & Shah, N. (2012). Applications of nano-catalyst in new era. *Journal Of Saudi Chemical Society*, *16*(3), 307-325. http://dx.doi.org/10.1016/j.jscs.2011.01.015

Chen, D., Qu, Z., Shen, S., Li, X., Shi, Y., & Wang, Y. et al. (2011). Comparative studies of silver based catalysts supported on different supports for the oxidation of formaldehyde. *Catalysis Today*, *175*(1), 338-345. doi:10.1016/j.cattod.2011.03.059

Chen, M. (2004). The Structure of Catalytically Active Gold on Titania. *Science*, *306*(5694), 252-255. doi:10.1126/science.1102420

Choi, T., & Hess, D. (2014). Chemical Etching and Patterning of Copper, Silver, and Gold Films at Low Temperatures. *ECS Journal Of Solid State Science And Technology*, *4*(1), N3084-N3093. doi:10.1149/2.0111501jss

Choi, T., & Hess, D. (2014). Chemical Etching and Patterning of Copper, Silver, and Gold Films at Low Temperatures. *ECS Journal Of Solid State Science And Technology*, *4*(1), N3084-N3093. doi:10.1149/2.0111501jss

Chou, S. Y., Krauss, P. R., & Renstrom, P. J. (1996). Nanoimprint lithography.*Journal of Vacuum Science & Technology B*, *14*(6), 4129-4133.

Chou, S., Krauss, P., & Renstrom, P. (1995). Imprint of sub-25 nm vias and trenches in polymers. *Appl. Phys. Lett.*, *67*(21), 3114. doi:10.1063/1.114851

Colburn, M., Johnson, S. C., Stewart, M. D., Damle, S., Bailey, T. C., Choi, B., ... & Willson, C. G. (1999, June). Step and flash imprint lithography: a new approach to high-resolution patterning. In *Microlithography'99* (pp. 379-389). International Society for Optics and Photonics.

Coq, B., & Figueras, F. (2003). Effects of particle size and support on some catalytic properties of metallic and bimetallic catalysts. *Catalysis and Electrocatalysis at Nanoparticle Surfaces*, 847-875.

Dutheil, P., Thomann, A., Lecas, T., Brault, P., & Vayer, M. (2015). Sputtered Ag thin films with modified morphologies: Influence on wetting property. *Applied Surface Science*, *347*, 101-108. doi:10.1016/j.apsusc.2015.04.052

Eichler, A., Kresse, G., & Hafner, J. (1998). Ab-initio calculations of the 6D potential energy surfaces for the dissociative adsorption of H2 on the (100) surfaces of Rh, Pd and Ag. *Surface Science*, *397*(1-3), 116-136. doi:10.1016/s0039-6028(97)00724-3

Escamilla-Perea, L., Nava, R., Pawelec, B., Rosmaninho, M., Peza-Ledesma, C., & Fierro, J. (2010). SBA-15-supported gold nanoparticles decorated by CeO2: Structural characteristics and CO oxidation activity. *Applied Catalysis A: General*, *381*(1-2), 42-53. doi:10.1016/j.apcata.2010.03.038

Fader, R., Schmitt, H., Rommel, M., Bauer, A., Frey, L., & Ji, R. et al. (2012). Novel organic polymer for UV-enhanced substrate conformal imprint lithography. *Microelectronic Engineering*, *98*, 238-241. doi:10.1016/j.mee.2012.07.010

Ferry, V., Verschuuren, M., Li, H., Schropp, R., Atwater, H., & Polman, A. (2009). Improved red-response in thin film a-Si:H solar cells with soft-imprinted plasmonic back reflectors. *Appl. Phys. Lett.*, *95*(18), 183503. doi:10.1063/1.3256187

Gao, W., Sattayasamitsathit, S., Manesh, K., Weihs, D., & Wang, J. (2010). Magnetically Powered Flexible Metal Nanowire Motors. *J. Am. Chem. Soc.*, *132*(41), 14403-14405. doi:10.1021/ja1072349

Gates, B., Xu, Q., Stewart, M., Ryan, D., Willson, C., & Whitesides, G. (2005). New Approaches to Nanofabrication: Molding, Printing, and Other Techniques. *Cheminform*, *36*(27). doi:10.1002/chin.200527216

Ge, X., Chen, L., Kang, J., Fujita, T., Hirata, A., & Zhang, W. et al. (2013). A Core-Shell Nanoporous Pt-Cu Catalyst with Tunable Composition and High Catalytic Activity. *Adv. Funct. Mater.*, *23*(33), 4156-4162. doi:10.1002/adfm.201300114

Glueckstein, J., Evans, M., & Nogami, J. (1996). Surface unwetting during growth of Ag on Si(001). *Phys. Rev. B*, *54*(16), R11066-R11069. http://dx.doi.org/10.1103/physrevb.54.r11066

Grass, R., Athanassiou, E., & Stark, W. (2007). Covalently Functionalized Cobalt Nanoparticles as a Platform for Magnetic Separations in Organic Synthesis. *Angewandte Chemie International Edition*, *46*(26), 4909-4912. doi:10.1002/anie.200700613

Grothausmann, R., Zehl, G., Manke, I., Fiechter, S., Bogdanoff, P., & Dorbandt, I. et al. (2011). Quantitative Structural Assessment of Heterogeneous Catalysts by Electron Tomography. *J. Am. Chem. Soc.*, *133*(45), 18161-18171. doi:10.1021/ja2032508

Grunwaldt, J., & Baiker, A. (1999). Gold/Titania Interfaces and Their Role in Carbon Monoxide Oxidation. *The Journal Of Physical Chemistry B*, *103*(6), 1002-1012. doi:10.1021/jp983206j

Haes, A., Zou, S., Schatz, G., & Van Duyne, R. (2004). Nanoscale Optical Biosensor:Â Short Range Distance Dependence of the Localized Surface Plasmon Resonance of Noble Metal Nanoparticles. *The Journal Of Physical Chemistry B*, *108*(22), 6961-6968. doi:10.1021/jp036261n

Han, A., Kuan, A., Golovchenko, J., & Branton, D. (2012). Nanopatterning on Nonplanar and Fragile Substrates with Ice Resists. *Nano Letters*, *12*(2), 1018-1021. doi:10.1021/nl204198w

Hansen, N., Ferguson, T., Panels, J., Park, A., & Joo, Y. (2011). Inorganic nanofibers with tailored placement of nanocatalysts for hydrogen production via alkaline hydrolysis of glucose. *Nanotechnology*, *22*(32), 325302. doi:10.1088/0957-4484/22/32/325302

Hariprasad, E., & Radhakrishnan, T. (2010). A Highly Efficient and Extensively Reusable “Dip Catalyst” Based on a Silver-Nanoparticle-Embedded Polymer Thin Film. *Chemistry - A European Journal*, *16*(48), 14378-14384. doi:10.1002/chem.201001679

Haruta, M. (1997). Size- and support-dependency in the catalysis of gold. *Catalysis Today*, *36*(1), 153-166. doi:10.1016/s0920-5861(96)00208-8

Heck, R., & Farrauto, R. (2001). Automobile exhaust catalysts. *Applied Catalysis A: General*, *221*(1-2), 443-457. doi:10.1016/s0926-860x(01)00818-3

Henriksen, T., Olsen, J., Vesborg, P., Chorkendorff, I., & Hansen, O. (2009). Highly sensitive silicon microreactor for catalyst testing. *Rev. Sci. Instrum.*, *80*(12), 124101. doi:10.1063/1.3270191

Henry, C. (2014). 2D-Arrays of Nanoparticles as Model Catalysts. *Catalysis Letters*, *145*(3), 731-749. http://dx.doi.org/10.1007/s10562-014-1402-6

Hohmeyer, J., Kondratenko, E., Bron, M., Kröhnert, J., Jentoft, F., Schlögl, R., & Claus, P. (2010). Activation of dihydrogen on supported and unsupported silver catalysts. *Journal Of Catalysis*, *269*(1), 5-14. doi:10.1016/j.jcat.2009.10.008

http://microchem.com/pdf/PMMA_Data_Sheet.pdf

http://www.cleanroom.byu.edu/wet_etch.phtml

Hua, J., Shao, M., Cheng, L., Wang, X., Fu, Y., & Ma, D. (2009). The fabrication of silver-modified silicon nanowires and their excellent catalysis in the decomposition of fluorescein sodium. *Journal Of Physics And Chemistry Of Solids*, *70*(1), 192-196. doi:10.1016/j.jpcs.2008.10.004

Huang, Y., Zhou, W., Hsia, K., Menard, E., Park, J., Rogers, J., & Alleyne, A. (2005). Stamp Collapse in Soft Lithography. *Langmuir*, *21*(17), 8058-8068. doi:10.1021/la0502185

Hwang, S., Jung, H., Jeong, J., & Lee, H. (2009). Fabrication of nano-sized metal patterns on flexible polyethylene-terephthalate substrate using bi-layer nanoimprint lithography. *Thin Solid Films*, *517*(14), 4104-4107. doi:10.1016/j.tsf.2009.01.164

JANKOWIAK, J., & BARTEAU, M. (2005). Ethylene epoxidation over silver and copperâ€“silver bimetallic catalysts: I. Kinetics and selectivity. *Journal Of Catalysis*, *236*(2), 366-378. doi:10.1016/j.jcat.2005.10.018

Ji, R., Hornung, M., Verschuuren, M., van de Laar, R., van Eekelen, J., & Plachetka, U. et al. (2010). UV enhanced substrate conformal imprint lithography (UV-SCIL) technique for photonic crystals

patterning in LED manufacturing. *Microelectronic Engineering*, *87*(5-8), 963-967. doi:10.1016/j.mee.2009.11.134

Jing, D., Ãœnal, B., Qin, F., Yuen, C., Evans, J., & Jenks, C. et al. (2009). Stranskiâ€"Krastanov-like growth of an Ag film on a metallic glass. *Thin Solid Films*, *517*(24), 6486-6492. http://dx.doi.org/10.1016/j.tsf.2009.03.203

Kapaklis, V., Poulopoulos, P., Karoutsos, V., Manouras, T., & Politis, C. (2006). Growth of thin Ag films produced by radio frequency magnetron sputtering. *Thin Solid Films*, *510*(1-2), 138-142. doi:10.1016/j.tsf.2005.12.311

Karimi, E., Vahdati-Khaki, J., Zebarjad, S., Bataev, I., & Bannov, A. (2014). A novel method for fabrication of Fe catalyst used for the synthesis of carbon nanotubes. *Bulletin Of Materials Science*, *37*(5), 1031-1038. doi:10.1007/s12034-014-0041-2

Kelkar, P., Beauvais, J., LavalleÌ• e, E., Drouin, D., Cloutier, M., & Turcotte, D. et al. (2004). Nano patterning on optical fiber and laser diode facet with dry resist. *Journal Of Vacuum Science & Technology A: Vacuum, Surfaces, And Films*, *22*(3), 743. doi:10.1116/1.1667503

Kim, Y., Park, N., Shin, J., Lee, S., Lee, Y., & Moon, D. (2003). Partial oxidation of ethylene to ethylene oxide over nanosized Ag/Î±-Al2O3 catalysts. *Catalysis Today*, *87*(1-4), 153-162. doi:10.1016/j.cattod.2003.09.012

Kolb, G., & Hessel, V. (2004). Micro-structured reactors for gas phase reactions. *Chemical Engineering Journal*, *98*(1-2), 1-38. doi:10.1016/j.cej.2003.10.005

Kooy, N., Mohamed, K., Pin, L., & Guan, O. (2014). A review of roll-to-roll nanoimprint lithography. *Nanoscale Res Lett*, *9*(1), 320. doi:10.1186/1556-276x-9-320

Kostovski, G., Chinnasamy, U., Jayawardhana, S., Stoddart, P., & Mitchell, A. (2011). Nanoimprinting: Sub-15nm Optical Fiber Nanoimprint Lithography: A Parallel, Self-aligned and Portable Approach (Adv. Mater. 4/2011). *Adv. Mater.*, *23*(4), 435-435. doi:10.1002/adma.201190003

Kuo, Y., & Lee, S. (2001). Room-temperature copper etching based on a plasma–copper reaction. *Appl. Phys. Lett.*, *78*(7), 1002. http://dx.doi.org/10.1063/1.1347388

Lee, H., Bien, D., Badaruddin, S., & Teh, A. (2012). Silver (Ag) as a novel masking material in glass etching for microfluidics applications. *Microsystem Technologies*, *19*(2), 253-259. http://dx.doi.org/10.1007/s00542-012-1574-1

Leech, P., Wu, N., & Zhu, Y. (2009). Application of dry film resist in the fabrication of microfluidic chips for droplet generation. *J. Micromech. Microeng.*, *19*(6), 065019. doi:10.1088/0960-1317/19/6/065019

Lewis, F. (1990). Solubility of hydrogen in metals. *Pure And Applied Chemistry*, *62*(11). doi:10.1351/pac199062112091

Li, X. (2012). Metal assisted chemical etching for high aspect ratio nanostructures: A review of characteristics and applications in photovoltaics. *Current Opinion In Solid State And Materials Science*, *16*(2), 71-81. doi:10.1016/j.cossms.2011.11.002

Li, X. (2012). Metal assisted chemical etching for high aspect ratio nanostructures: A review of characteristics and applications in photovoltaics. *Current Opinion In Solid State And Materials Science*, *16*(2), 71-81. doi:10.1016/j.cossms.2011.11.002

Liang, J., Kohsaka, F., Matsuo, T., Li, X., & Ueda, T. (2008). Improved bi-layer lift-off process for MEMS applications. *Microelectronic Engineering*, *85*(5-6), 1000-1003. doi:10.1016/j.mee.2008.01.104

Liang, X., Tan, H., Fu, Z., & Chou, S. Y. (2007). Air bubble formation and dissolution in dispensing nanoimprint lithography. *Nanotechnology*, *18*(2), 025303.

Lin, R., Liu, W., Zhong, Y., & Luo, M. (2001). Catalyst characterization and activity of Ag–Mn complex oxides. *Applied Catalysis A: General*, *220*(1-2), 165-171. doi:10.1016/s0926-860x(01)00718-9

Lin, S. D., & Vannice, M. A. (1993). Hydrogenation of aromatic hydrocarbons over supported Pt catalysts. I. Benzene hydrogenation. *Journal of Catalysis*,*143*(2), 539-553.

Linic, S., & Barteau, M. A. (2003). Construction of a reaction coordinate and a microkinetic model for ethylene epoxidation on silver from DFT calculations and surface science experiments. *Journal of Catalysis*, *214*(2), 200-212.

Linic, S., Jankowiak, J., & Barteau, M. (2004). Selectivity driven design of bimetallic ethylene epoxidation catalysts fromÂ first principles. *Journal Of Catalysis*, *224*(2), 489-493. doi:10.1016/j.jcat.2004.03.007

Lippits, M., Gluhoi, A., & Nieuwenhuys, B. (2007). A comparative study of the effect of addition of CeO x and Li2O on Î³-Al2O3 supported copper, silver and gold catalysts in the preferential oxidation of CO. *Topics In Catalysis*, *44*(1-2), 159-165. doi:10.1007/s11244-007-0289-5

Liu, H., Ma, D., Blackley, R., Zhou, W., & Bao, X. (2008). Highly active mesostructured silica hosted silver catalysts for CO oxidation using the one-pot synthesis approach. *Chemical Communications*, (23), 2677. doi:10.1039/b804641g

Liu, R., An, F., Zhang, S., Luo, J., & Liu, X. (2013). Photosensitive acrylate copolymer for electrodeposition photoresist. *Polym. Sci. Ser. A*, *55*(4), 225-232. doi:10.1134/s0965545x13040093

Luisetto, I., Pepe, F., & Bemporad, E. (2008). Preparation and characterization of nano cobalt oxide. *Journal Of Nanoparticle Research*, *10*(S1), 59-67. doi:10.1007/s11051-008-9365-4

Manfrinato, V., Wen, J., Zhang, L., Yang, Y., Hobbs, R., & Baker, B. et al. (2014). Determining the Resolution Limits of Electron-Beam Lithography: Direct Measurement of the Point-Spread Function. *Nano Letters*, *14*(8), 4406-4412. http://dx.doi.org/10.1021/nl5013773

Manfrinato, V., Zhang, L., Su, D., Duan, H., Hobbs, R., Stach, E., & Berggren, K. (2013). Resolution Limits of Electron-Beam Lithography toward the Atomic Scale. *Nano Letters*, 130321102652000. doi:10.1021/nl304715p

Manheller, M., Trellenkamp, S., Waser, R., & Karthäuser, S. (2012). Reliable fabrication of 3 nm gaps between nanoelectrodes by electron-beam lithography. *Nanotechnology*, *23*(12), 125302. doi:10.1088/0957-4484/23/12/125302

Maraghechi, P., Cadien, K., & Elezzabi, A. (2011). A Novel Nanofabrication Damascene Lift-Off Technique. *IEEE Transactions On Nanotechnology*, *10*(4), 822-826. doi:10.1109/tnano.2010.2081374

Martinez-Duarte, R., Teixidor, G. T., Mukherjee, P. P., Kang, Q., & Madou, M. J. (2010). Perspectives of micro and nanofabrication of carbon for electrochemical and microfluidic applications. In *Microfluidics and Microfabrication* (pp. 181-263). Springer US.

Mashaiekhy, J., Shafieizadeh, Z., & Nahidi, H. (2012). Effect of substrate temperature and film thickness on the characteristics of silver thin films deposited by DC magnetron sputtering. *Eur. Phys. J. Appl. Phys.*, *60*(2), 20301. http://dx.doi.org/10.1051/epjap/2012120212

Metin, O., Mazumder, V., OÌˆzkar, S., & Sun, S. (2010). Monodisperse Nickel Nanoparticles and Their Catalysis in Hydrolytic Dehydrogenation of Ammonia Borane. *J. Am. Chem. Soc.*, *132*(5), 1468-1469. doi:10.1021/ja909243z

Moshfegh, A. (2009). Nanoparticle catalysts. *Journal Of Physics D: Applied Physics*, *42*(23), 233001. doi:10.1088/0022-3727/42/23/233001

Muñoz, J., Cervantes, J., Esparza, R., & Rosas, G. (2007). Iron nanoparticles produced by high-energy ball milling. *Journal Of Nanoparticle Research*, *9*(5), 945-950. doi:10.1007/s11051-007-9226-6

Nagy, A., Mestl, G., & Schlögl, R. (1999). The Role of Subsurface Oxygen in the Silver-Catalyzed, Oxidative Coupling of Methane. *Journal Of Catalysis*, *188*(1), 58-68. doi:10.1006/jcat.1999.2651

Narayanan, R. (2005). *SHAPE-DEPENDENT NANOCATALYSIS AND THE EFFECT OF CATALYSIS ON THE SHAPE AND SIZE OF COLLOIDAL METAL NANOPARTICLES* (PHD). Georgia Institute of Technology.

Narkiewicz, U., Podsiadły, M., Arabczyk, W., Woźniak, M., & Kurzydłowski, K. (2007). Carbon-coated cobalt nanoparticles. *Materials Science And Engineering: C*, *27*(5-8), 1273-1276. doi:10.1016/j.msec.2006.08.026

Ohama, Y., & Van Gemert, D. (Eds.). (2011). *Application of Titanium Dioxide Photocatalysis to Construction Materials: State-of-the-art Report of the RILEM Technical Committee 194-TDP* (Vol. 5). Springer Science & Business Media.)

Ojur, J., Ahmad, F., & Haris, M. (2013). CMOS Compatible Bulk Micromachining. *Advances In Micro/Nano Electromechanical Systems And Fabrication Technologies*. doi:10.5772/55526

Okumura, M., Nakamura, S., Tsubota, S., Nakamura, T., Azuma, M., & Haruta, M. (1998). Chemical vapor deposition of gold on Al2O3, SiO2, and TiO2 for the oxidation of CO and of H2. *Catalysis Letters*, *51*(1-2), 53-58.

PÃ¢rvulescu, V., Cojocaru, B., PÃ¢rvulescu, V., Richards, R., Li, Z., & Cadigan, C. et al. (2010). Solâ€“gel-entrapped nano silver catalysts-correlation between active silver species and catalytic behavior. *Journal Of Catalysis*, *272*(1), 92-100. doi:10.1016/j.jcat.2010.03.008

Pârvulescu, V., Cojocaru, B., Pârvulescu, V., Richards, R., Li, Z., & Cadigan, C. et al. (2010). Sol–gel-entrapped nano silver catalysts-correlation between active silver species and catalytic behavior. *Journal Of Catalysis*, *272*(1), 92-100. doi:10.1016/j.jcat.2010.03.008

Philippot, K., & Serp, P. (2013). Concepts in nanocatalysis. *Nanomaterials in Catalysis*, 1-54.

Prathyusha, T., Reddy, C. S., Reddy, P. S., & Reddy, A. S. Effect of sputtering power on the properties of dc magnetron sputtered Au-SnO2 films.

Raffi, M., Akhter, J., & Hasan, M. (2006). Effect of annealing temperature on Ag nano-composite synthesized by solâ€“gel. *Materials Chemistry And Physics*, *99*(2-3), 405-409. doi:10.1016/j.matchemphys.2005.11.012

Rahman, I., Vejayakumaran, P., Sipaut, C., Ismail, J., Abu Bakar, M., Adnan, R., & Chee, C. (2006). Effect of anion electrolytes on the formation of silica nanoparticles via the sol–gel process. *Ceramics International*, *32*(6), 691-699. doi:10.1016/j.ceramint.2005.05.004

RAKOCEVIC, Z., PETROVIC, R., & STRBAC, S. (2008). Surface roughness of ultra-thin silver films sputter depositedon a glass. *Journal Of Microscopy*, *232*(3), 595-600. doi:10.1111/j.1365-2818.2008.02123.x

Ren, L., Zhang, H., Lu, A., Hao, Y. and Li, W. (2012). Porous silica as supports for controlled fabrication of Au/CeO2/SiO2 catalysts for CO oxidation: Influence of the silica nanostructures. *Microporous and Mesoporous Materials*, 158, pp.7-12.

Richter, M., Bentrup, U., Eckelt, R., Schneider, M., Pohl, M. M., & Fricke, R. (2004). The effect of hydrogen on the selective catalytic reduction of NO in excess oxygen over Ag/Al 2 O 3. *Applied Catalysis B: Environmental*, *51*(4), 261-274.

Rizzo, A., Tagliente, M., Alvisi, M., & Scaglione, S. (2001). Structural and optical properties of silver thin films deposited by RF magnetron sputtering. *Thin Solid Films*, *396*(1-2), 29-35. doi:10.1016/s0040-6090(01)01242-1

Roucoux, A., Schulz, J., & Patin, H. (2002). Reduced Transition Metal Colloids:Â A Novel Family of Reusable Catalysts?. *Chemical Reviews*, *102*(10), 3757-3778. doi:10.1021/cr010350j

Sanada, T., Murakami, C., GÃ³ra-Marek, K., Iida, K., Katada, N., & Okumura, K. (2013). Fabrication and Catalytic Activity of Thermally Stable Gold Nanoparticles on Ultrastable Y (USY) Zeolites. *Catalysts*, *3*(3), 599-613. doi:10.3390/catal3030599

Sardar, R., Funston, A., Mulvaney, P., & Murray, R. (2009). Gold Nanoparticles: Past, Present, and Future â€ . *Langmuir*, *25*(24), 13840-13851. doi:10.1021/la9019475

Schmitt, H., Duempelmann, P., Fader, R., Rommel, M., Bauer, A., & Frey, L. et al. (2012). Life time evaluation of PDMS stamps for UV-enhanced substrate conformal imprint lithography. *Microelectronic Engineering*, *98*, 275-278. http://dx.doi.org/10.1016/j.mee.2012.04.032

Scirè, S., Crisafulli, C., Giuffrida, S., Mazza, C., Riccobene, P., & Pistone, A. et al. (2009). Supported silver catalysts prepared by deposition in aqueous solution of Ag nanoparticles obtained through a photochemical approach. *Applied Catalysis A: General*, *367*(1-2), 138-145. doi:10.1016/j.apcata.2009.07.046

Scirè, S., Riccobene, P., & Crisafulli, C. (2010). Ceria supported group IB metal catalysts for the combustion of volatile organic compounds and the preferential oxidation of CO. *Applied Catalysis B: Environmental*, *101*(1-2), 109-117. doi:10.1016/j.apcatb.2010.09.013

Sekine, Y. (2002). Oxidative decomposition of formaldehyde by metal oxides at room temperature. *Atmospheric Environment*, *36*(35), 5543-5547. doi:10.1016/s1352-2310(02)00670-2

Seyedmonir, S. R., Strohmayer, D. E., Geoffroy, G. L., Vannice, M. A., Young, H. W., & Linowski, J. W. (1984). Characterization of supported silver catalysts: I. Adsorption of O2, H2, N2O, and the H2-titration of adsorbed oxygen on well-dispersed Ag on TiO2. *Journal of Catalysis*, *87*(2), 424-436.

Shen, Y., Yao, L., Li, Z., Kou, J., Cui, Y., & Bian, J. et al. (2013). Double transfer UV-curing nanoimprint lithography. *Nanotechnology*, *24*(46), 465304. doi:10.1088/0957-4484/24/46/465304

Shin, K., Cho, Y., Choi, J., & Kim, K. (2012). Facile synthesis of silver-deposited silanized magnetite nanoparticles and their application for catalytic reduction of nitrophenols. *Applied Catalysis A: General*, *413-414*, 170-175. doi:10.1016/j.apcata.2011.11.006

Shin, K., Choi, J., Park, C., Jang, H., & Kim, K. (2009). Facile Synthesis and Catalytic Application of Silver-Deposited Magnetic Nanoparticles. *Catalysis Letters*, *133*(1-2), 1-7. doi:10.1007/s10562-009-0124-7

Soltani, M., Lin, J., Forties, R., Inman, J., Saraf, S., & Fulbright, R. et al. (2014). Nanophotonic trapping for precise manipulation of biomolecular arrays. *Nature Nanotech*, *9*(6), 448-452. doi:10.1038/nnano.2014.79

Srivastava, S., Kumar, D., Vandana, Sharma, M., Kumar, R., & Singh, P. (2012). Silver catalyzed nano-texturing of silicon surfaces for solar cell applications. *Solar Energy Materials And Solar Cells*, *100*, 33-38. http://dx.doi.org/10.1016/j.solmat.2011.05.003

Stamenkovic, V., Mun, B., Arenz, M., Mayrhofer, K., Lucas, C., & Wang, G. et al. (2007). Trends in electrocatalysis on extended and nanoscale Pt-bimetallic alloy surfaces. *Nature Materials*, *6*(3), 241-247. doi:10.1038/nmat1840

Sultana, S. (2010). RF magnetron sputtering system. *Centre for Excellence in Nano-Electronics Indian Institute of Science, Bangalore-12*.

Takenaka, S., Kobayashi, S., Ogihara, H., & Otsuka, K. (2003). Ni/SiO 2 catalyst effective for methane decomposition into hydrogen and carbon nanofiber. *Journal of Catalysis*, *217*(1), 79-87.

Tang, C. C., & Hess, D. W. (1984). Tungsten Etching in CF 4 and SF 6 Discharges. *Journal of the Electrochemical Society*, *131*(1), 115-120.

Tian, N., Zhou, Z., Sun, S., Ding, Y., & Wang, Z. (2007). Synthesis of Tetrahexahedral Platinum Nanocrystals with High-Index Facets and High Electro-Oxidation Activity. *Cheminform*, *38*(31). doi:10.1002/chin.200731015

Tsukuda, T., Tsunoyama, H., & Sakurai, H. (2011). Aerobic Oxidations Catalyzed by Colloidal Nanogold. *Chem. Asian J.*, *6*(3), 736-748. doi:10.1002/asia.201000611

Valden, M., Lai, X., & Goodman, D. W. (1998). Onset of catalytic activity of gold clusters on titania with the appearance of nonmetallic properties. *Science*,*281*(5383), 1647-1650.

van Delft, F., van de Laar, R., Verschuuren, M., Platzgummer, E., & Loeschner, H. (2010). Charged Particle Nanopatterning (CHARPAN) of 2D and 3D masters for flexible replication in Substrate Conformal Imprint Lithography (SCIL). *Microelectronic Engineering*, *87*(5-8), 1062-1065. doi:10.1016/j.mee.2009.11.088

Veith, G., Lupini, A., Rashkeev, S., Pennycook, S., Mullins, D., & Schwartz, V. et al. (2009). Thermal stability and catalytic activity of gold nanoparticles supported on silica. *Journal Of Catalysis*, *262*(1), 92-101. doi:10.1016/j.jcat.2008.12.005

Verschuuren, M. (2010). *Substrate Conformal Imprint Lithography for Nanophotonics* (PhD). Utrecht University.

Vershuuren, M., & van Sprang, H. (2012). Large-area nanopatterns: improving LEDs, lasers, and photovoltaics. *SPIE Newsroom*. http://dx.doi.org/10.1117/2.1201206.004248

Wang, H., & Liu, C. (2011). Preparation and characterization of SBA-15 supported Pd catalyst for CO oxidation. *Applied Catalysis B: Environmental*, *106*(3-4), 672-680. doi:10.1016/j.apcatb.2011.06.034

Wang, X., Ji, H., Zhang, X., Zhang, H., & Yang, X. (2010). Hollow polymer microspheres containing a gold nanocolloid core adsorbed on the inner surface as a catalytic microreactor. *J Mater Sci*, *45*(15), 3981-3989. doi:10.1007/s10853-010-4470-z

Wang, Z., Yan, J., Wang, H., & Jiang, Q. (2013). Self-protective cobalt nanocatalyst for long-time recycle application on hydrogen generation by its free metal-ion conversion. *Journal Of Power Sources*, *243*, 431-435. doi:10.1016/j.jpowsour.2013.05.193

Wei, H., Gomez, C., Liu, J., Guo, N., Wu, T., & Lobo-Lapidus, R. et al. (2013). Selective hydrogenation of acrolein on supported silver catalysts: A kinetics study of particle size effects. *Journal Of Catalysis*, *298*, 18-26. doi:10.1016/j.jcat.2012.10.027

Wojcieszak, R., Monteverdi, S., Ghanbaja, J., & Bettahar, M. (2008). Study of Ni–Ag/SiO2 catalysts prepared by reduction in aqueous hydrazine. *Journal Of Colloid And Interface Science*, *317*(1), 166-174. doi:10.1016/j.jcis.2007.09.031

Wu, B., Kumar, A., & Pamarthy, S. (2010). High aspect ratio silicon etch: A review. *J. Appl. Phys.*, *108*(5), 051101. doi:10.1063/1.3474652

Xia, Y., & Whitesides, G. M. (1998). Soft lithography. *Annual review of materials science*, *28*(1), 153-184.

Xiong, Y., Wu, H., Guo, Y., Sun, Y., Yang, D., & Da, D. (2000). Preparation and characterization of nanostructured silver thin films deposited by radio frequency magnetron sputtering. *Thin Solid Films*, *375*(1-2), 300-303. http://dx.doi.org/10.1016/s0040-6090(00)01253-0

Xu, X., Tang, Z., Shao, J., & Fan, Z. (2005). The study on the interface adhesion comparison of the MgF2, Al2O3, SiO2 and Ag thin films. *Applied Surface Science*, *245*(1-4), 11-15. http://dx.doi.org/10.1016/j.apsusc.2004.10.018

Yamada, Y., Yano, K., & Fukuzumi, S. (2012). Catalytic application of shape-controlled Cu 2 O particles protected by Co 3 O 4 nanoparticles for hydrogen evolution from ammonia borane. *Energy Environ. Sci.*, *5*(1), 5356-5363. doi:10.1039/c1ee02639a

Yan, J., Zhang, X., Shioyama, H., & Xu, Q. (2010). Room temperature hydrolytic dehydrogenation of ammonia borane catalyzed by Co nanoparticles. *Journal Of Power Sources*, *195*(4), 1091-1094. doi:10.1016/j.jpowsour.2009.08.067

Yimsiri, P., & Mackley, M. (2006). Spin and dip coating of light-emitting polymer solutions: Matching experiment with modelling. *Chemical Engineering Science*, *61*(11), 3496-3505. doi:10.1016/j.ces.2005.12.018

Yuan, K., Yu, B., & Pan, D. (2012). E-Beam Lithography Stencil Planning and Optimization With Overlapped Characters. *IEEE Transactions On Computer-Aided Design Of Integrated Circuits And Systems*, *31*(2), 167-179. doi:10.1109/tcad.2011.2179041

Zarraga-Colina, J., & Nix, R. (2006). Fabrication of model Pt-ceria catalysts and an analysis of their performance for CO oxidation. *Surface Science*, *600*(15), 3058-3071. doi:10.1016/j.susc.2006.05.047

Zhang, C., He, H., & Tanaka, K. (2005). Perfect catalytic oxidation of formaldehyde over a Pt/TiO2 catalyst at room temperature. *Catalysis Communications*, *6*(3), 211-214. doi:10.1016/j.catcom.2004.12.012

Zhang, G., Tanii, T., Zako, T., Hosaka, T., Miyake, T., & Kanari, Y. et al. (2005). Nanoscale Patterning of Protein Using Electron Beam Lithography of Organosilane Self-Assembled Monolayers. *Small*, *1*(8-9), 833-837. doi:10.1002/smll.200500091

Zhang, J., Con, C., & Cui, B. (2014). Electron Beam Lithography on Irregular Surfaces Using an Evaporated Resist. *ACS Nano*, *8*(4), 3483-3489. doi:10.1021/nn4064659

Zhang, L., Dou, Y., & Gu, H. (2006). Synthesis of Ag–Fe3O4 heterodimeric nanoparticles. *Journal Of Colloid And Interface Science*, *297*(2), 660-664. doi:10.1016/j.jcis.2005.11.009

Zhang, Q., Li, J., Liu, X., & Zhu, Q. (2000). Synergetic effect of Pd and Ag dispersed on Al2O3 in the selective hydrogenation of acetylene. *Applied Catalysis A: General*, *197*(2), 221-228. doi:10.1016/s0926-860x(99)00463-9

Zhang, Y., Janyasupab, M., Liu, C., Li, X., Xu, J., & Liu, C. (2012). Three Dimensional PtRh Alloy Porous Nanostructures: Tuning the Atomic Composition and Controlling the Morphology for the Application of Direct Methanol Fuel Cells. *Adv. Funct. Mater.*, *22*(17), 3570-3575. doi:10.1002/adfm.201200678

Zhou, Z., Kooi, S., Flytzani-Stephanopoulos, M., & Saltsburg, H. (2008). The Role of the Interface in CO Oxidation on Au/CeO 2 Multilayer Nanotowers. *Adv. Funct. Mater.*, *18*(18), 2801-2807. doi:10.1002/adfm.200800025

Zhukov, V., Rendulic, K., & Winkler, A. (1996). Coadsorption of hydrogen and potassium on silver single crystal surfaces. *Vacuum*, *47*(1), 5-11. doi:10.1016/0042-207x(95)00181-6

List of Figures

Figure 1 shows the "EHE" pattern was decomposed into 11 rectangles and then required total 11 shots (Yuan, Yu & Pan, 2012) .... Error! Bookmark not defined.

Figure 2shows a comparison between standard UV NIL and thermal NIL processes 35

Figure 3 shows difference between (a) isotropic and (b) anisotropic wet etching 38

Figure 4 shows one of the standard patterns designed especially for this experiment 46

Figure 5 displays the spin speed versus film thickness curve 49

Figure 6 present the array features onto thick PMMA layer 49

Figure 7 shows the two rows of dots array imprinted onto C1%PMMA 51

Figure 8 SEM scan displays the 10nm Ag thin film with A) some grains of random size and shape, and B) unclear features 52

Figure 9 SEM scan shows dots patterns onto SiO2 surface: A) 100nm spacing of 6 time main dose. B) 150nm spacing of 16 times main does. C) 200nm spacing of 24 times main dose. (100 nm spacing) x6 base dose (150 nm spacing) x16 base dose (200 nm spacing) x24 base 53

Figure 10 SEM scan shows the patterns on 20nm AG thin film deposited onto SiO2 with various dose exposures. A) Factor 1. B) Factor 2. C) Factor 3. D) Factor 4. 55

Figure 11 SEM scan explains for: A) 150nm spacing of 16 times base dose exposure. B) 200nm spacing of 24 times base dose. C) 200nm spacing of 36 times base dose. 55

Figure 12 shows sample surface, PMMA residuals and irregular Ag patterns by employing lift off method with C4%PMMA 57

Figure 13 presents SEM scans for nanostructures after lift-off C1%PMMA photoresist: A) 50nm spacing of 10 dose factor. B) 100nm spacing of 10 dose factor. C) 50nm spacing of 20 dose factor. D) 100nm spacing of 20 dose factor. E) 150nm spacing of 20 dose factor. F) 200nm spacing of 20 dose factor. G) 50nm spacing of 22 dose factor. H) 50 & 100 nm spacing of 40 dose factor. 59

Figure 14 displays XPS spectrum for surface compositions after lift-off process 62

Figure 15 shows a photographic image for the master wafer after cleaning with visible patterns 65

Figure 16 photographic images show the effect of the anti-sticking layer FDTS on DI water droplets. 66

Figure 17 displays the rubber stamp on a glass sheet with a black rubber ring 67

Figure 18 illustrates schematically the basic steps for the substrate conformal imprint lithography technique (Vershuuren & van Sprang, 2012) 69

Figure 19 presents the final appearance of the imprinted wafer at 100µm gap 70

Figure 20 shows the final appearance of the imprinted wafer at 90µm gap 70

Figure 21 SEM images for: A) perfect SiNW, (B&C) a microchannel with defects 72

Figure 22 evaluates the dimension measurements for most SiNWs measured by the aid of SEM skills 73

Figure 23 displays the cross section analyses by SEM: A) one end of a microchannel with its pad B) zoom in the channel cross section C) the resist thickness remained on features D) the total thickness of the deposited resist 74

List of Tables

Table 1 shows a few AgNPs/ supports to advance catalysis reactions 11
Table 2 shows PtNPs as an example of shape dependent catalysis 11
Table 3 shows (gold/ceria/silica) as an example of materials dependent catalysis 12
Table 4 shows some available examples of size dependent catalysis 12
Table 5 Comparison of silver properties with respect to gold and copper 14
Table 6 shows the most common deposition methods used in the configuration of catalysts 28
Table 7 shows the conditions of depositing 10 nm silver layer 44
Table 8 shows the conditions of depositing 20 nm silver layer 47
Table 9 summarises the replication steps of SCIL 4”- Stamp 71